

INVESTIGATION OF OIL-INJECTED SCREW COMPRESSORS PERFORMANCE
BASED ON ENERGY EFFICIENCY AND PRESSURIZED AIR QUALITY



by
Şükrü Erikli

Submitted to Graduate School of Natural and Applied Sciences
in Partial Fulfillment of the Requirements
for the Degree of Master of Science in
Mechanical Engineering

Yeditepe University
2017

INVESTIGATION OF OIL-INJECTED SCREW COMPRESSORS PERFORMANCE
BASED ON ENERGY EFFICIENCY AND PRESSURIZED AIR QUALITY

APPROVED BY:

Assist. Prof. Dr. Ali Bahadır Olcay
(Thesis Supervisor)




.....

Prof. Dr. Erdem Hojin Ahn



.....

Assist. Prof. Dr. Murat Sarıbay



.....

DATE OF APPROVAL:/...../2017

ACKNOWLEDGEMENTS

It is with immense gratitude that I acknowledge the support and help of my advisor, Assistant Professor Ali Bahadır OLCAY. Pursuing my thesis under his supervision has been a productive experience which broadens the mind and presents an unlimited source of learning. Also I want to express special thanks to Prof. Doctor Mehmet Alaeddin AKGÜN for his support in my academic and professional career.

Finally, I would like to thank my family members, Recep ERİKLİ, Selma ERİKLİ, Ender ERİKLİ and Ebru ERİKLİ for their endless love and support, what makes everything more beautiful.

ABSTRACT

INVESTIGATION OF OIL-INJECTED SCREW COMPRESSORS PERFORMANCE BASED ON ENERGY EFFICIENCY AND PRESSURIZED AIR QUALITY

Energy consumption of a compressor can constitute almost 40% of the overall energy consumption of a facility. Screw compressors are the most common type of compressors. The main function of the bare screw compressor is to pressurize gas. While the gas is being compressed in a pressure chamber of an oil injected screw compressor, gas temperature causes entropy generation. So, some oil is injected into the pressure chamber as a coolant. This oil injection also provides lubrication for rotors and decreases leakages. This study covers the calculation of oil injection port locations and injection nozzle diameters based on the cooling effects of oil on air.

This study also investigates hydrocyclone performance of an oil injected screw compressor. Hydrocyclones cover a significant portion of overall energy performance and the oil separation efficiency of a screw compressor is significant for air quality. As a result of their complex flow structure they cannot be modelled with algebraic methods. Therefore, numerical CFD methods are preferred for the purpose of the estimation of hydrocyclone flow. Modelling a hydrocyclone with CFD needs more extended study compared to modelling a cyclone.

In this study, three separation efficiency parameters of hydrocyclone are investigated, i.e., vortex finder location, inlet diameter and flow volume height between oil reservoir surface and top of the hydrocyclone. With regard to separation and energy performance, thirteen different cases have been investigated which are cyclone inlet diameter and flow volume height between oil reservoir surface and top surface of oil. The reversed vortex generation was observed at various cross-sectional planes of flow volume of the tank. The inlet diameter of the cyclone proved to be related to the centrifugal force on particles, so decrease in diameter means faster inflow; and a larger diameter implies slower inflow. On the contrary, increment in the flow speed causes breakup problems, causing the particle diameters to get smaller; consequently, separating particles from gas becomes harder.

ÖZET

YAĞ ENJEKTELI VIDALI KOMPRESÖRLERİN ENERJİ VERİMLİLİĞİ VE BASINÇLI HAVA KALİTESİ BAZ ALINARAK İNCELENMESİ

Kompresörlerin tükettiği enerji bir tesisin toplam enerji tüketiminin %40 na ulaşabilir. Piyasada en çok tercih edilen vidalı kompresörlerin verimini en çok etkileyen parçalar vida ünitesi ve hidrosiklon tanklarıdır. Yağ enjekteli vida ünitesi içerisinde havanın basınçlandırılması esnasında ısı açığa çıkar. Belirli sıcaklığa ulaşan basınç odasındaki hava üzerine yağ enjeksiyonu yapılarak soğutma sağlanır. Enjeksiyon noktasındaki sıcaklığın belirlenmesi, enjeksiyon deliklerinin çapları ve bunlara bağımlı birçok değişkenin gözlemlenmesi temel tasarım kriterlerini oluşturur. Bu çalışmada bu tasarım kriterleri ele alınacaktır.

Bu çalışmada hidrosiklon ayırıcıların yağ enjekteli kompresörlerin performansları üzerindeki etkileri incelenmiştir. Hidrosiklonların verimliliği tüm sistem performansı içerisinde genellikle önemli bir yer tutar. Bilgisayar sistemlerinin hem donanımsal hem de yazılımsal olarak gelişmesiyle birlikte yüksek girdaplı akışlar, HAD (Hesaplamalı Akışkanlar Dinamiği) yazılımları yardımıyla çözülebilmektedir. Hidrosiklonların HAD ile modellenmesi siklonlarla kıyasla çok daha kapsamlı bir çalışma gerektirir.

Bu çalışmada, yağ enjekteli vidalı kompresörlerin hidrosiklonlarında girdap akış çizgilerinin oluşmasında büyük rol oynayan vorteks yakalayıcı kanalın yatay eksende konumu, hidrosiklonların giriş çapının ve akış hacminin ayrıştırma ve enerji performansı üzerindeki etkileri HAD yöntemiyle incelenmiştir. Bu parametrelerin çeşitli kombinasyonlarından oluşan on üç farklı durum modellenerek sonuçlar gözlemlenmiştir. Bu parametrelerin ayrıştırılacak partiküllerin üzerine etkileyen kuvvetler üzerinde güçlü bir etkisi olduğu gözlemlenmiş ve optimizasyon teknikleri raporlanmıştır.

TABLE OF CONTENTS

ACKNOWLEDGEMENTS.....	iii
ABSTRACT.....	iv
ÖZET	v
LIST OF FIGURES	vii
LIST OF TABLES.....	x
LIST OF SYMBOLS/ABBREVIATIONS.....	xi
1. INTRODUCTION	1
2. THERMODYNAMIC ANALYSIS OF A BARE OIL-INJECTED SCREW COMPRESSOR.....	9
2.1. OIL INJECTION PORT LOCATION ON Z AXIS.....	14
2.2. OIL VOLUMETRIC FLOW RATE FROM OIL INJECTION NOZZLE	22
2.3. OIL INJECTION NOZZLE DIAMETER.....	26
3. INLET DIAMETER AND FLOW VOLUME EFFECTS ON THE SEPARATION AND ENERGY EFFICIENCY OF HYDROCYCLONES.....	30
3.1. NUMERICAL MODEL.....	30
3.2. VALIDATION OF NUMERICAL MODEL OF OIL SEPARATION TANK ..	37
4. INVESTIGATION OF VORTEX FINDER LOCATION EFFECTS ON ENERGY AND SEPARATION EFFICIENCY ON HYDROCYCLONES	44
4.1. GEOMETRY OF SIMULATED VORTEX FINDER POSITIONS	45
4.2. NUMERICAL MODEL.....	50
4.3. SIMULATION RESULTS.....	50
5. CONCLUSIONS	57
6. REFERENCES	59

LIST OF FIGURES

Figure 1.1. Chart of basic compressor types.....	2
Figure 1.2. Schematics of Oil Injected Screw Compressors.....	4
Figure 1.3. 3D model with air and oil flow animation of an oil injected screw compressor.	4
Figure 1.4. A typical oil injected screw compressor.....	5
Figure 1.5. A vertical oil separation tank.....	6
Figure 2.1. Oil injected screw compressor 3D model shows rotors in casing.....	9
Figure 2.2. Isometric view for the next figure temperature and pressure increment contours	10
Figure 2.3. Temperature and pressure contours on rotors	11
Figure 2.4. Temperature and pressure increment in pressure chamber in case of no oil injection	12
Figure 2.5. Thermodynamic approach to bare oil injected screw compressor unit	13
Figure 2.6. Calculation results of ambient temperature vs. air pressure in pressure chamber at oil injection port location	15
Figure 2.7. Calculation results of oil injection temperature vs. air pressure in pressure chamber at oil injection port location	16
Figure 2.8. Coordinate System Z1 and Z2 axes.....	17

Figure 2.9. Calculation results of ambient air temperature vs. oil port location on Z axis..	18
Figure 2.10. Calculation results of oil injection temperature vs. oil port location on Z axis	19
Figure 2.11. The estimated location of the oil injection ports on Z axis (Volumetric change of the pressure chamber was calculated with Solidworks.)	21
Figure 2.12. Calculation results and experimental observation of required oil injection flow rate vs. discharge air temperature	23
Figure 2.13. Calculation results of discharge Air Temperature vs. Oil Injection Temperature	24
Figure 2.14. Thermodynamic schematic of standard cooling system of air end	25
Figure 2.15. Calculation results of oil injection hole diameter vs oil injection flow rate....	29
Figure 3.1. Numerical model with parameters	32
Figure 3.2. Numerical model with computational grid.....	33
Figure 3.3. Pressure loss variations with inlet velocity for Gao's experimental and numerical studies and current study.....	39
Figure 3.4. Tangential velocities on the line parallel to the Z axis at the 75 mm offset from $y = 0$ (a) at inlet velocity of 15.2 m/s (b) at inlet velocity of 16.9 m/s (c) at inlet velocity of 18.1 m/s.....	41
Figure 3.5. Pressure loss variations with different inlet duct height and swirl volume height	42
Figure 3.6. Separation efficiency with different inlet duct height and swirl volume height	43

Figure 4.1. Separation efficiency with different inlet duct and swirl volume height	45
Figure 4.2. Parameters of oil tank geometry.....	46
Figure 4.3. Mesh Overview	47
Figure 4.4. Contours of velocity magnitude (m/s) at 0° vortex finder position.....	51
Figure 4.5. Contours of velocity magnitude (m/s) at 180° vortex finder position.....	52
Figure 4.6. Contours of velocity magnitude (m/s) at 90° vortex finder position.....	53
Figure 4.7. Contours of velocity magnitude (m/s) at 270° vortex finder position.....	54
Figure 4.8. Pressure loss values for different off centred vortex positions	55
Figure 4.9. Particle separation efficiency values for different off centred vortex positions	56

LIST OF TABLES

Table 1.1. Comparison table of basic types of screw compressors	3
Table 2.1. Air properties	20
Table 2.2. Air properties for oil injection temperature calculation	25
Table 2.3. Air properties for oil injection flow rate calculation	26
Table 2.4. Table of oil injection particle and nozzle properties	27
Table 2.5. Table of oil particle properties for nozzle diameter calculation	28
Table 2.6. Result list of oil injection nozzle diameter calculation.....	28
Table 3.1. Hydrocyclone geometric parameters	30
Table 3.2. Grid independency check results	31
Table 3.3. Studied cases (total of nine different models was generated for the study)	32
Table 3.4. Pressure loss variations with inlet velocity for Gao's experimental and numerical studies and current study.....	38
Table 4.1. Parameters of Oil Separation Tank.....	45
Table 4.2. Grid independency check results	48
Table 4.3. Number of meshes	48

LIST OF SYMBOLS/ABBREVIATIONS

a	Hydrocyclone inlet duct height
b	Hydrocyclone inlet duct width
b_{crit}	Break-up constant
$c_p(T)$	Specific heat capacity at corresponding temperature
C_{D_0}	Drag coefficient of a particle
d	Particle diameter
d_0	Particle initial diameter
D	Hydrocyclone diameter
f	Term is related to the ratio between particles radius.
$h_{in(air)}$	Enthalpy of air at suction port temperature
$h_{in(oil)}$	Enthalpy of oil at injection temperature
$h_{out(air)}$	Enthalpy air at outlet port
$h_{out(oil)}$	Enthalpy of oil at outlet
H	Swirl volume height
h	Hydrocyclone central duct height
l_p	Characteristic length of particle
L	Hydrocyclone central duct inlet length
m_1	1 st particle mass
m_2	2 nd particle mass
$\dot{m}_{in(air)}$	Air mass input
$\dot{m}_{in(oil)}$	Injected oil mass flow rate
P	Pressure
\dot{Q}	Dissipated heat with body of air end
r_1	1 st particle radius
r_2	2 nd particle radius
R	Specific gas constant
s^o	Specific entropy
T	Temperature
t	Time

t_d	Characteristic time of droplet deformation
Δt	Time step interval
u_p	Particle velocity
u_p^n	Particle internal velocity
u_p^{n+1}	Particle calculated velocity
u	Medium velocity
v	Particle swimming velocity in air medium
v'_1	Coalescent particle velocity
We	Weber number
We_c	Critical weber number
$\dot{W}_{in(mechanical)}$	Mechanical work provided to the male rotor
$\dot{W}_{(Mechanical Losses)}$	Mechanical losses of bearings, friction between rotors or friction between rotors and casing on axial direction
x_p^n	Particle initial location
x_p^{n+1}	Particle calculated location
$y(t)$	Dependent value of break-up terms for estimation break-up moment
Y	Random number between 0 and 1
ρ_p	Particle density
σ_p	Particle surface tension
τ_p	Shear stress on particle surface
ω	Growth rate of the perturbation
DPM	Discrete phase model
eff	Efficiency in %
RSM	Reynolds stress model
TAB	Taylor Analogy Breakup

1. INTRODUCTION

Compressors are devices used for pressurizing gases, and pressurized gas is preferred for many purposes like gas transportation, power transmission or energy storage [1] [2]. Moreover, about 40% of the world's energy is consumed by compressors [3]. As pneumatic systems are cheaper than other systems and potential energy can be stored with them for many years without any loss, they are mainly preferred for power transmission [4]. Other energy storage methods lose energy proportional to storage time.

The main problem with pressurizing gasses is related to entropy generation; because when a volume of gas is pressurized, the increase in gas temperature causes entropy generation [5]. According to ideal gas theory, as the temperature increases, the pressure rises as well. While the gas is being compressed, the pressure generated from temperature increment decreases efficiency of process. For this reason, chamber cooling system is an important design criterion for compressors.

There are different types of compressors [6]. The most efficient compressor type can only be selected by considering the pressure and users capacity needs [7]. Compressors can be classified as positive displacement and dynamic compressors according to their pressurizing technique as seen in Figure 1.1. Dynamic compressors increase the kinetic energy of gas, than it converts kinetic energy to potential energy. Common models of dynamic compressors are axial and radial compressors. Positive displacement compressors fill gas in a chamber, and then decrease the volume of chamber. A reduction in the chamber volume causes increase in the air pressure. This study focuses on screw compressors under the category of positive displacement compressors.

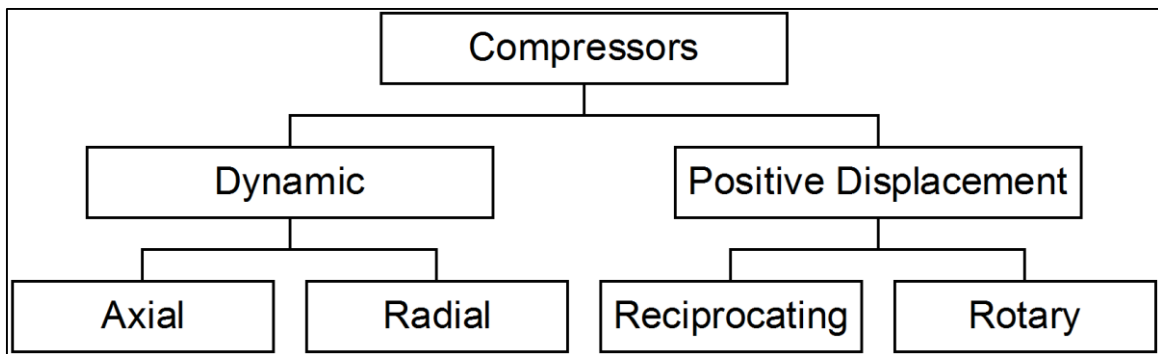


Figure 1.1. Chart of basic compressor types

Nowadays the screw compressor units are commonly used to pressurize air for factories [8]. Thanks to their low maintenance costs and high efficiency, screw compressors are feasible for investment. Many different types of screw compressors are available for the alternating facility needs. Main compressor types are oil injected, dry and water injected screw compressors. The cooling system plays a significant role in the efficiency of a compressor and there are various compressor cooling systems in the market. These systems have both advantages and disadvantages regarding to the costs of investment and maintenance.

The most widespread type of screw compressors are oil-injected screw compressors thanks to their feasibility in terms of their price and efficiency [9] [10]. The other common types of screw compressors are oil-free and water injected screw compressors. The main problem with the oil-injected screw compressors is that while gas is being compressed, some oil is injected into the pressure chamber as a coolant [11]. The pressurized gas goes to a special separator system in order to purify gas from oil particles. Although there are advanced separation systems, their cost is too high to be used in a compressor system [12]. So, generally basic separation systems are preferred, but it is not possible to provide the system with completely oil free air by using a regular cost-effective separation system. Therefore, the engineering of a screw compressor requires a design with no oil coolant injection. There are two options for such a design; firstly, the coolant injection feature can be left out, and secondly, another liquid can be used as the coolant.

The oil-free screw compressors are designed with cooling jackets like an engine. These cooling jackets are a good solution, but the cooling method is not as efficient as injection method. Besides, they require higher temperatures than injection cooling technique [13]. For compressors, the higher temperature means a shorter life span and more maintenance

intervals, and also requires expensive sealing elements with a special design, and working parts with higher tolerance as well.

Water injected screw compressors use water as a coolant liquid [14], [15], [16]. Working with water is really challenging, because it has specific properties; it has a corrosive nature, its density varies with the changes in temperature and its boiling point is too low. Despite all these effects, heat capacity of water is higher than other coolants and it can be seen as the best liquid as coolant. Although water injected compressors are the most efficient type of screw compressors, they are the most expensive ones.

To sum up, compressor types can be compared as in the table below in terms of their efficiency, investment and maintenance cost, and preference rate.

Table 1.1. Comparison table of basic types of screw compressors

	Efficiency	Investment Cost	Maintenance Cost	Most Preferred
1st	Water injected	Oil-free	Oil-free	Oil injected
2nd	Oil injected	Water injected	Water injected	Oil-free
3rd	Oil-free	Oil injected	Oil injected	Water injected

A screw compressor is formed from the combination of several sub-systems as illustrated in Figure 1.2-1.3-1.4 [17]. This study emphasizes the factors affecting the performance of oil-injected screw compressors. Performance of these compressors is mostly affected by sub-systems like suction system, bare screw compressor unit, separation system, drive unit, and cooling system of radiator as shown in Figure 1.2. The functions of these systems can be explained as follows: the main role of the suction system is to provide filtered clean air to the bare screw compressor with sound absorbing capability. Bare screw compressor unit's role is to compress air with high efficiency [18]. Separation system separates oil from pressurized air with minimum pressure loss and maximum separation efficiency. Drive unit generates torque from electricity with maximum efficiency and stability [19]. Lastly, the cooling system cools down air and oil temperatures with minimum pressure loss [20]. In this study, bare screw compressor unit and separation system, which are the essential components, will be examined and outlet values of other sub systems will be reported.

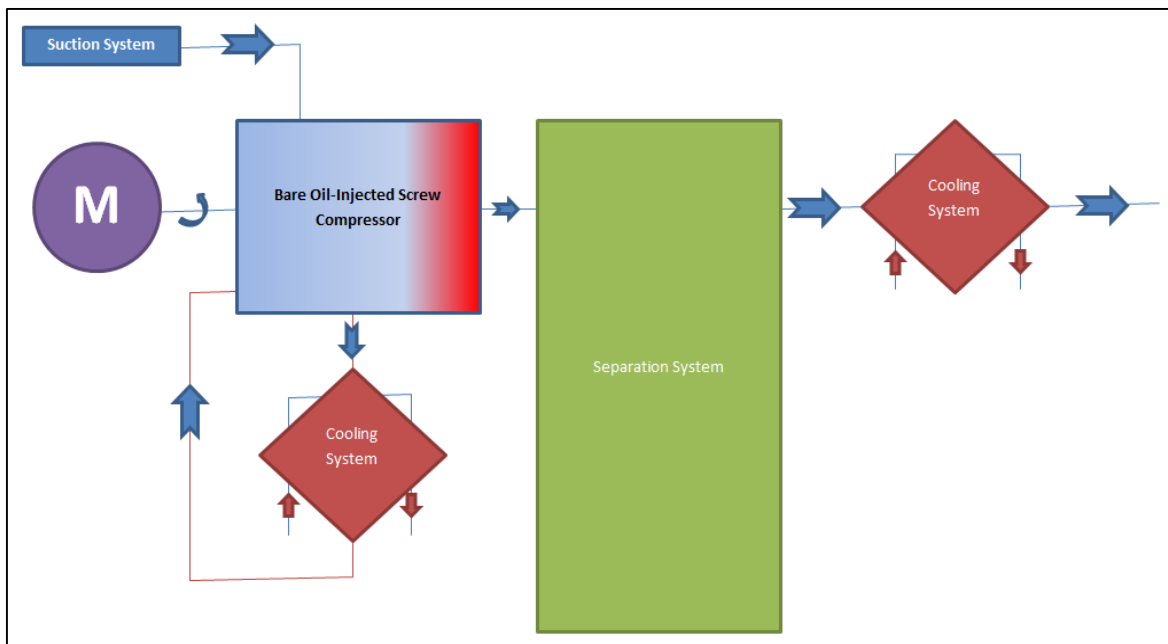


Figure 1.2. Schematics of Oil Injected Screw Compressors

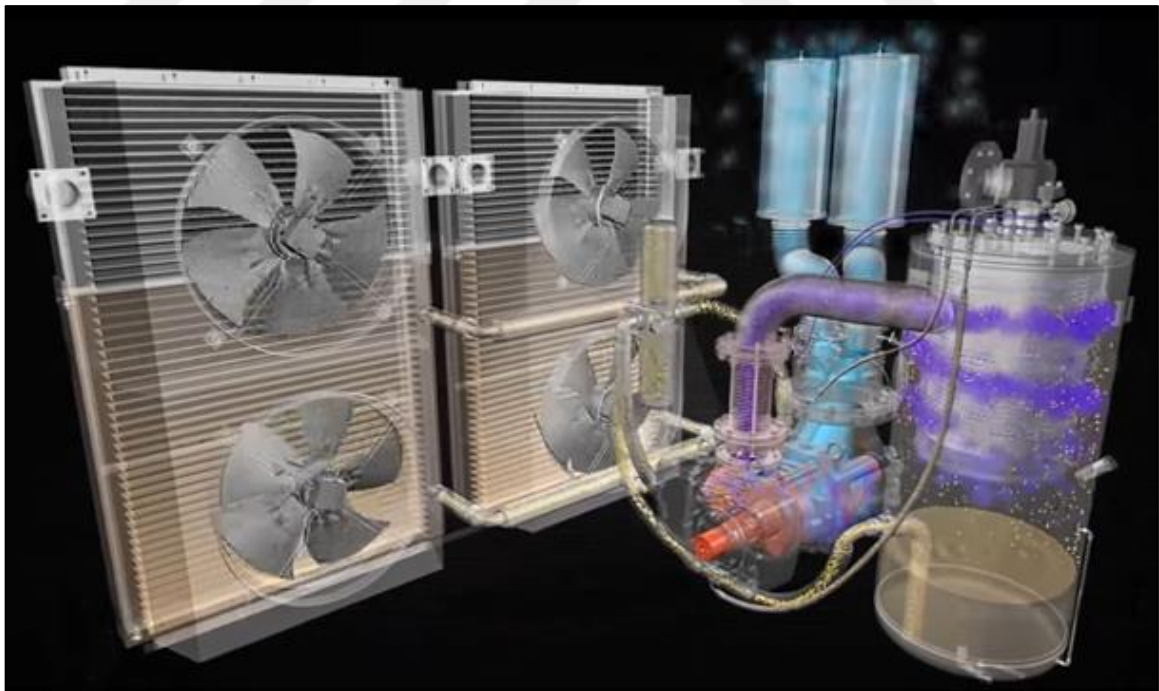


Figure 1.3. 3D model with air and oil flow animation of an oil injected screw compressor

The most important design considerations for a bare screw compressor unit in terms of efficiency are oil injection port locations, the volumetric flow rate of oil from oil injection, and the diameter of the oil injection nozzle [13], [21]–[23]. To understand the individual effects of these parameters on energy consumption, relation between these parameters will be investigated.



Figure 1.4. A typical oil injected screw compressor

Another important factor on the performance is the oil separator tank (Figure 1.5). It may be assumed to be the largest component of an oil injected screw compressor. Its main function is to separate oil from the air-oil mixture. However, if the design of a separator is not properly done, the oil cannot be separated from air perfectly; besides, the total pressure loss of separation stage becomes higher than it is supposed to be.



Figure 1.5. A vertical oil separation tank

Basic separation system of oil-injected screw compressors consists of two parts. One of them is cyclone separator and the other one is coalescence separator. Cyclones known as separators are commonly used to extract particles or droplets from the system with the help of centrifugal forces. Furthermore, cyclone structures can be easily manufactured and they have low maintenance and investment costs. While these advantages make the cyclone systems quite popular in the industry, their complex flow characteristics with swirls cannot

be solved with mathematical models. Therefore, experimental or numerical approaches have been used to determine the performance of the cyclones. There are many experimental studies regarding to the design of cyclone systems [24]–[26]. However, experimental approaches have their own difficulties to identify the flow inside the cyclone since visualization of entire fluid flow inside a closed geometry is very challenging. Hence, observations from inlet and outlet measurements have been typically used to quantify performance parameters of these systems while numerical studies can help to understand the flow characteristics in cyclone systems. As a result of improvements in the computer processors and solver programs, the time needed to complete a numerical solution has been decreasing; therefore, nowadays many numerical studies [27]–[29] related to fluid flow in cyclone systems can be found.

As the fluid flow inside cyclone systems is inherently turbulent, the studies about the turbulence model for swirling flows [29] are examined. It was realized that while the Reynolds Stress Model (RSM) has been widely accepted for swirling flows in these studies, Reynolds Averaged Navier-Stokes (RANS) has been generally employed for fluid flow simulations since this method gives results with more reasonable errors [30] compared to Large Eddy Simulation (LES) solutions.

In addition to fluid flow simulations in cyclone systems, the particles can be essentially observed with two different methods, namely volume of fluid (VOF) and discrete phase method (DPM). The oil reservoir at the bottom of the oil tank and desired number of particles can be modelled in VOF method despite certain restrictions. The limitations in VOF model can be mainly summarized as the need for longer computational time in VOF than in DPM method. The VOF method's inability to model the surface tension or velocity on the droplet surface. On the other hand, DPM is a simulation technique widely used for particle flows and with DPM method particles can be traced and monitored. Besides, different particle models such as collision of particles or particle break up can be employed. Studies [31] show that the DPM results in cyclone modelling become more accurate with Euler-Lagrangian approach.

When flow characteristics of cyclones and hydrocyclones are considered, gas flow characteristics are observed to be the same for both systems while the particle characteristics display some differences. Particularly, while dust cyclones are used to separate solid particles such as dusts, hydrocyclones are utilized for separation of liquids from gas flow.

When solid particles flow in the gas phase, there is no change in the shape of solid particles whereas the shape of liquid particles in gas flow can change due to speed, pressure, or the specification of a gas [32]. However, there is a common challenge for cyclones and hydrocyclones that small particles are typically hard to be separated from large particles. There are many studies regarding to dust cyclone geometries and turbulence models used in these studies which can be employed for hydrocyclones; however, studies about particles are not applicable for hydrocyclones. When the fluid flow speed becomes large enough, the liquid droplets break up and start to flow as small droplets; as a result, the high speed in hydrocyclones becomes an undesirable situation. On the other hand, collision of solid particles can be interpreted as elastic collisions while the liquid particle collision causes both coalescence and elastic collision. After a collision, the particle diameter increases, and if the particle diameter passes the already set critical diameter value, the particle may break up into smaller particles. Therefore, the breakup and coalescence effects must be considered for hydrocyclones [33]. The breakup effect on the separation performance has been studied by Gao et al. [34] extensively.

The cyclone geometry has been investigated by different researchers. The famous experimental studies based on dust cyclones are examined again with different methods or simulations [28]. Noroozil et al. [35] not only investigated the effects of the cyclone inlet diameter on cyclone performance, but also the inlet port angle of the cyclone. The impacts of the cyclone main body diameter on its own performance was studied by Yetilmezsoy, 2006 [36].

In this study, inlet diameter and flow volume effects on the separation and energy efficiency of hydrocyclones were simulated and investigated. Simulation was based on the RANS method. The particles were traced with the DPM method and the coalescence and breakup effects were considered. In case of decreasing the inlet diameter causes to increase breakup rate of droplets and the smaller droplets can separate from flow harder. Decreasing the diameter of the main [37] body of the cyclone increases the pressure drop.. The optimum dimension rate between main body and inlet diameter was found and discussed.

2. THERMODYNAMIC ANALYSIS OF A BARE OIL-INJECTED SCREW COMPRESSOR

The main performance factors of a compressor are generally related to cooling strategy (Figure 2.1). The critical points for performance can be predicted as oil injection location, oil injection temperature, oil injection nozzle diameters and oil injection flow rate [38] [39].

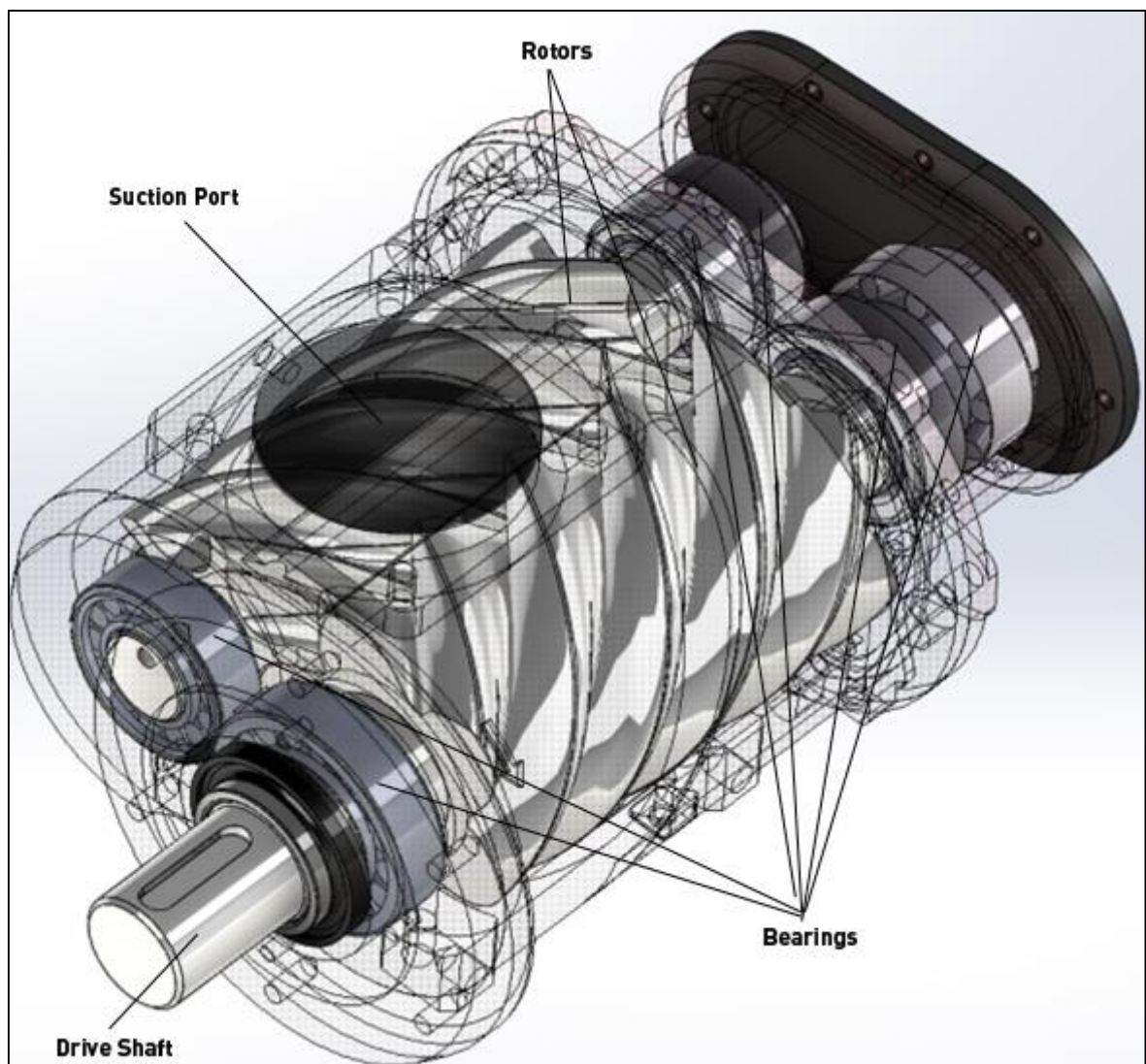


Figure 2.1. Oil injected screw compressor 3D model shows rotors in casing

The oil injection port location is related to stage pressure chambers in bare screw compressor unit. The bare compressor unit sucks air from atmosphere and starts to compress it. Each lobe of rotors can be assumed as a pressure chamber. As the gas goes to the discharge port,

gas pressure in lobes increases step by step. Total leakage between lobes of rotors in the compression process decreases drastically since lobe stages retard the escaping air from high to low pressure sides. According to the ideal gas theory, temperature changes in proportional to pressure (Figure 2.2-2.3) (values shown in Figure 2.2 and Figure 2.3 are calculated with the basic ideal gas formula). Oil injection temperature must be near or lower than the gas temperature in the pressure chamber [39] [40]. For this reason, its location is important, because temperature is a dependent. If the oil injection temperature is higher than the temperature in the chamber, then gas within the chamber warms up earlier than supposed to be. Therefore, its pressure increases and starts to consume more mechanical power. If the oil injection temperature is lower than the chamber temperature, the oil injection ports gets closer to discharge port, therefore duration of the oil existence in the chamber will not enough for efficient heat transfer from gas to oil. As a result, the location of injection ports was seen to be critical for cooling performance.

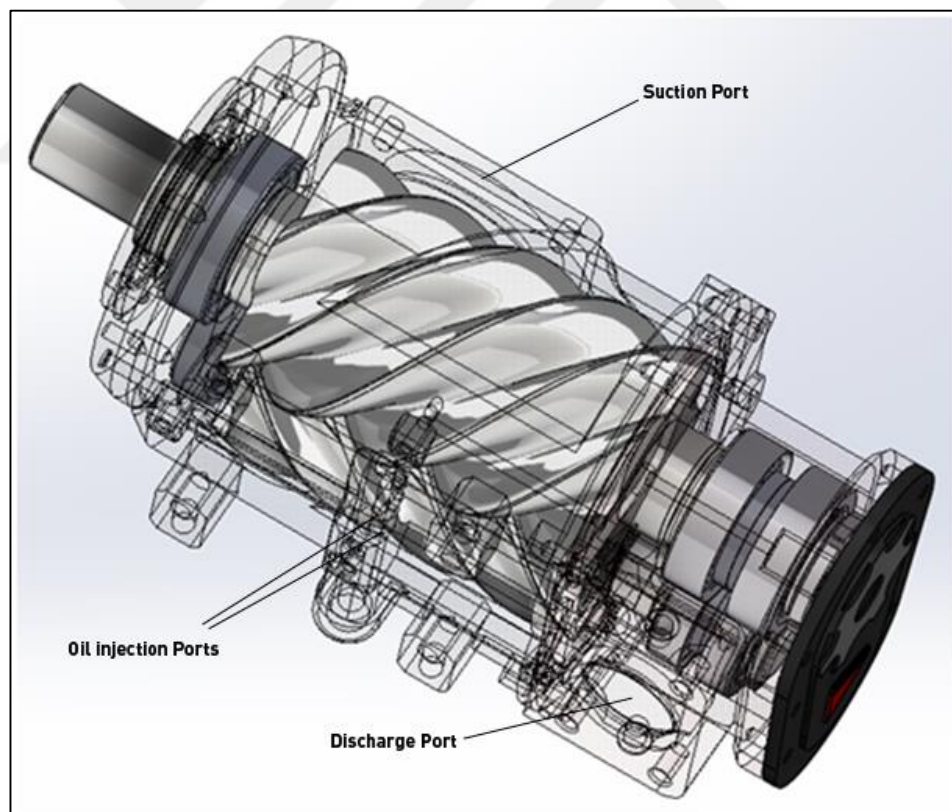


Figure 2.2. Isometric view for the next figure temperature and pressure increment contours

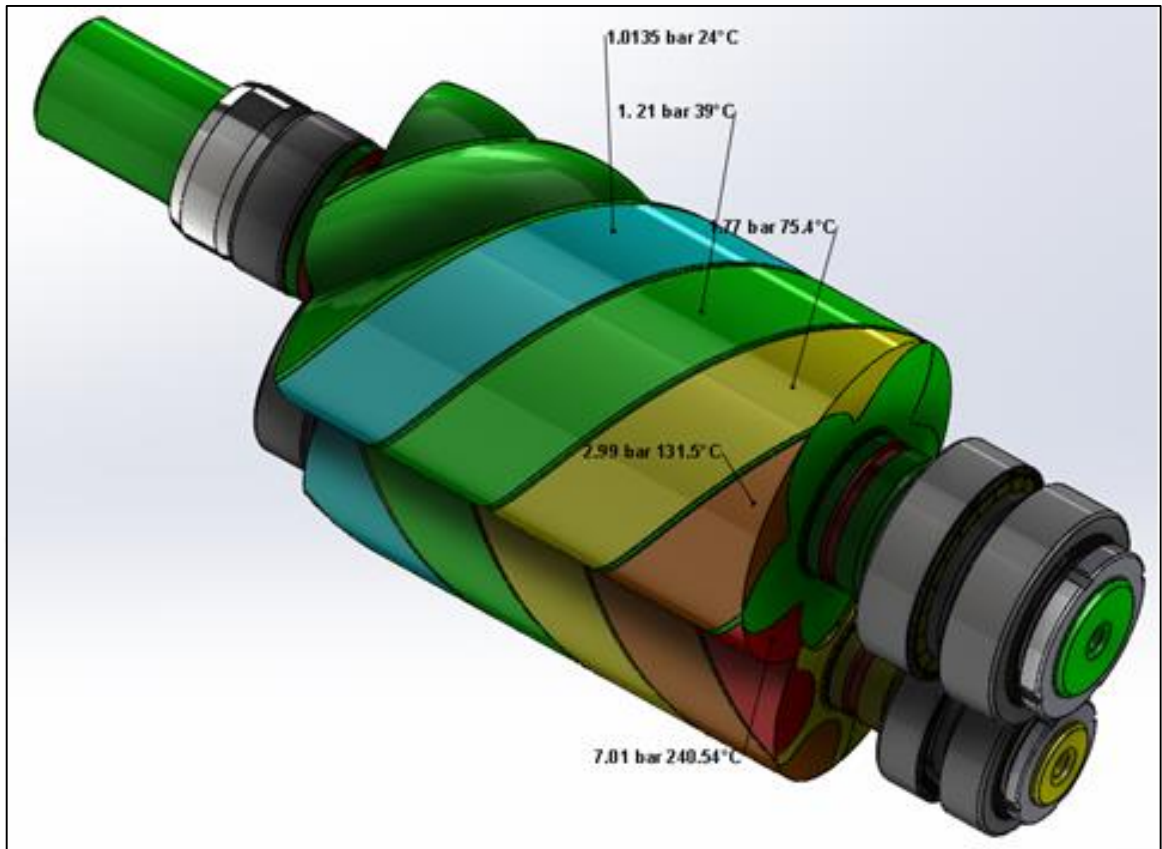


Figure 2.3. Temperature and pressure contours on rotors

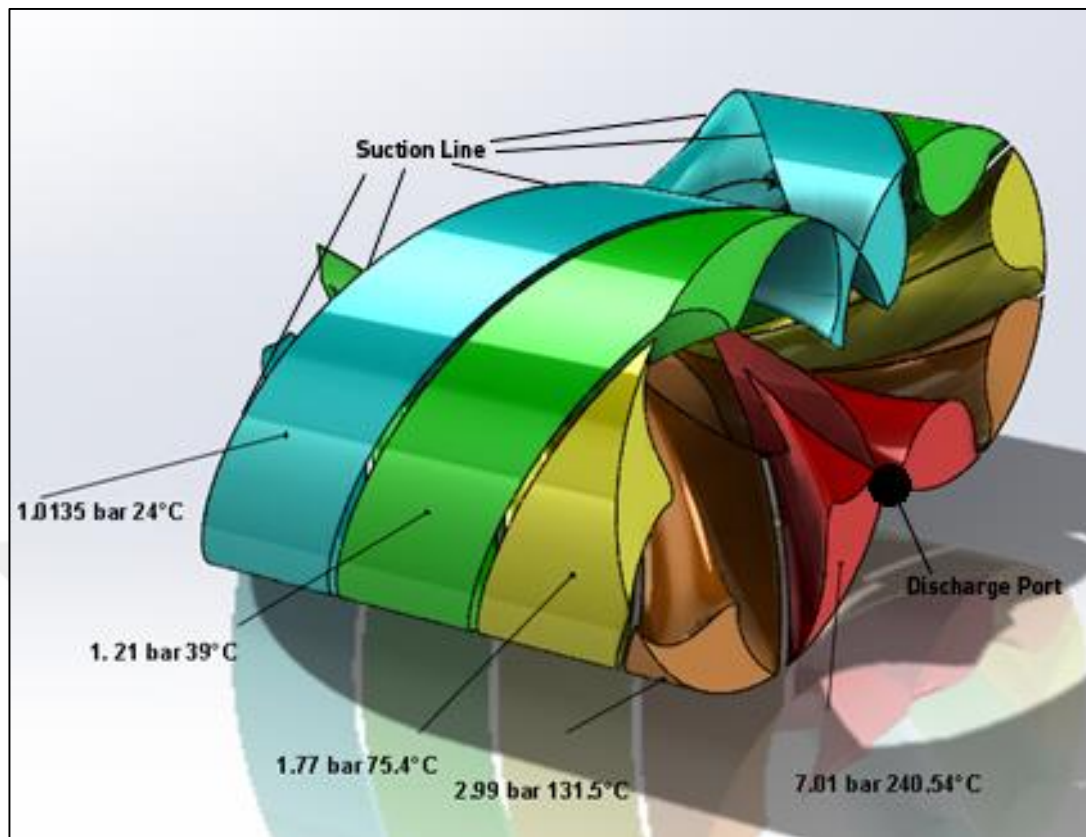


Figure 2.4. Temperature and pressure increment in pressure chamber in case of no oil injection

Another important factor of cooling performance is atomizing performance of nozzles. It is directly related to the function of oil injection nozzle diameters, chamber pressure and oil injection flow rate [40]. During the observation of cooling with injection, it must always be kept in mind that injected oil particles stay in pressure chamber only for 0.005 seconds. So, the atomizing performance is quite sensitive due to this short duration. In case of greater oil injection port diameter, the atomized particles of oil do not have enough surface area; therefore, the interaction between oil and gas in terms of heat transfer is not enough for efficient cooling [41]. Besides, heavy particles directly stick to rotors. If the oil injection ports are smaller than they should be, then the oil is atomized to very small particles. As a result of the insufficient mass of particles, the centrifugal force of air flow causes the oil particles to stick to outer surface of the pressure chamber [40].

The clearance between rotors and the gap between housing and rotors are as small as 0.005 mm [42], [43].

The most important design points for a bare screw compressor unit in terms of efficiency are oil injection port locations, oil volumetric flow rate from oil injection, and oil injection nozzle diameter [44]. The dependency between these parameters is examined and the individual effects of these parameters on performance will be presented with curves.

For an oil injected screw compressor, thermodynamic efficiency system can be drawn as below (Figure 2.5).

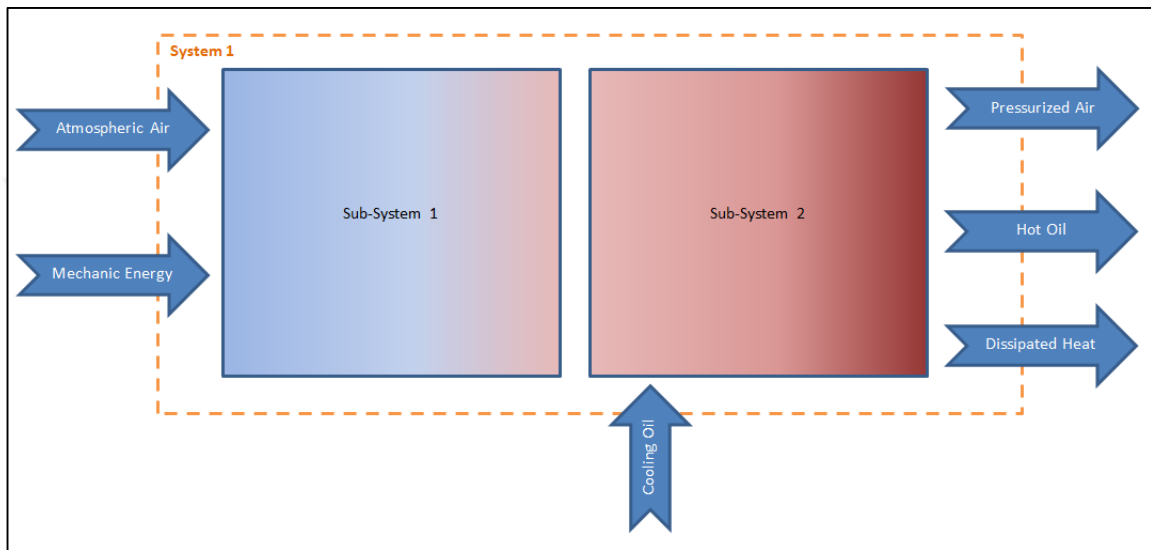


Figure 2.5. Thermodynamic approach to bare oil injected screw compressor unit

The energy equality of a screw compressor for an open system can be formulated as below.

$$\dot{m}_{in(air)} + \dot{m}_{in(oil)} = \dot{m}_{out(air)} + \dot{m}_{out(oil)} \quad (2.1)$$

$$\begin{aligned} \dot{W}_{in(mechanical)} + \dot{m}_{in(air)}h_{in(air)} + \dot{m}_{in(oil)}h_{in(oil)} \\ = \dot{m}_{out(air)}h_{out(air)} + \dot{m}_{out(oil)}h_{out(oil)} + \dot{Q} \\ + \dot{W}_{(Mechanical Losses)} \end{aligned} \quad (2.2)$$

Here, $\dot{W}_{in(mechanical)}$ represents mechanical work provided to the male rotor, $\dot{m}_{in(air)}$ is volume of the air mass sucked by airoend, $\dot{m}_{in(oil)}$ indicates injected oil mass , $h_{in(air)}$ symbolizes enthalpy of air at suction port temperature, $h_{in(oil)}$ is enthalpy of oil at injection temperature. $\dot{m}_{out(air)}$ represents the quantity of air at discharge port and $\dot{m}_{out(oil)}$ is the

quantity of oil at discharge port. $h_{out(air)}$ indicates enthalpy of pressurized air at outlet port, $h_{out(oil)}$ is enthalpy of oil at outlet. \dot{Q} is dissipated heat with body of airend and $\dot{W}_{(Mechanical Losses)}$ shows mechanical losses of bearings, friction between rotors or friction between rotors and casing on axial direction. In order to calculate the needed mechanical energy, the energy of discharged air and discharged oil must be measured. Besides, dissipated heat and mechanical losses generally consumes 10% percent of total energy, but in this study they are totally ignored [45].

2.1. OIL INJECTION PORT LOCATION ON Z AXIS

In order to increase energy efficiency of the airend, oil should be injected at the location where pressurized air temperature becomes the same with the oil injection temperature [46]. Ambient temperature is one of the factor of air temperature value in the chamber at the oil injection port location. If the suction air temperature is increased, the pressurized air temperature reaches to the oil injection temperature earlier. The effects of ambient temperature are simply calculated according to the ideal gas theory. Figure 2.6 shows how the air pressure changes with the ambient temperature.

$$P * V = n * R * \Delta T \quad (2.3)$$

Oil injection temperature and ambient temperature are assumed to be constant, so s_1 and s_2 are known values. P_1 is the ambient temperature and P_2 represents the air pressure at the oil injection port location.

$$s_2 = s_1 + R * \ln \left(\frac{P_2}{P_1} \right) \quad (2.4)$$

Equation 2.4 is iterated for different oil injection and ambient temperatures. The results are shown in Figure 2.6 and Figure 2.7.

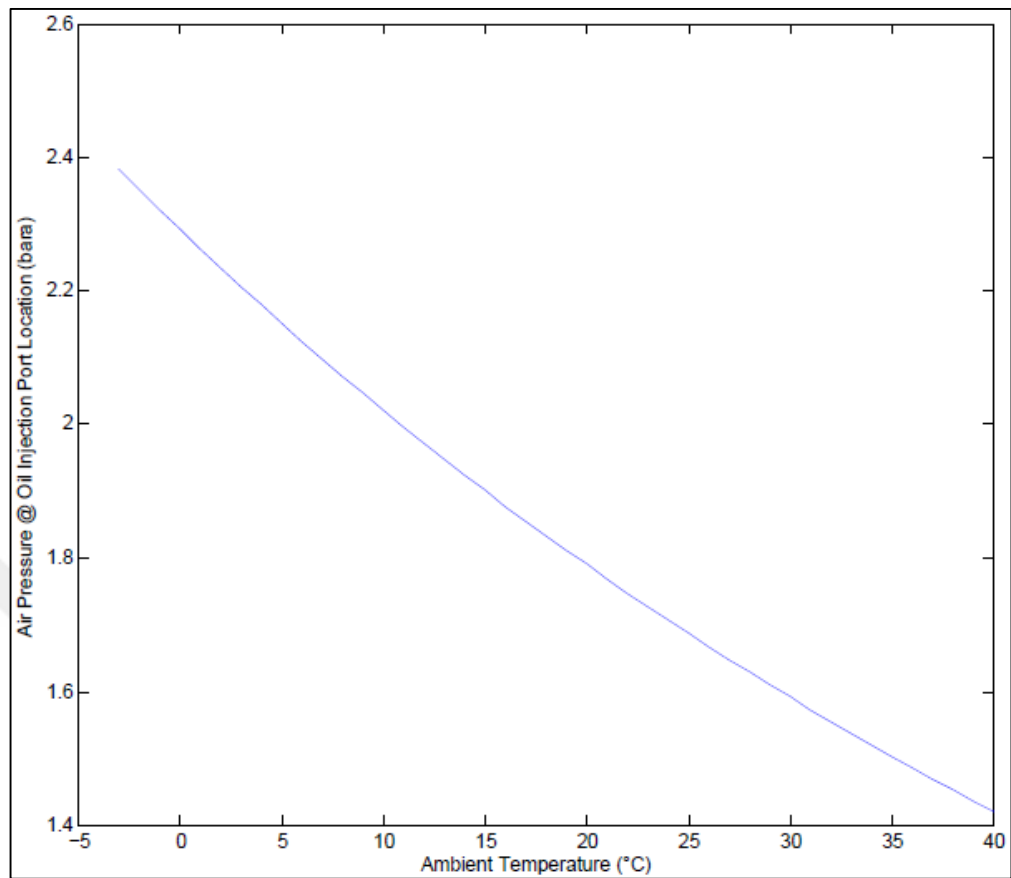


Figure 2.6. Results for ambient temperature vs. air pressure in pressure chamber at oil injection port location

Oil injection temperature is related to chamber pressure at oil injection location (Figure 2.6). The temperature equality between air and the injected oil is significant, because oil stays in pressure chamber is so short that heat transfer duration between air and oil is in delicate balance state.

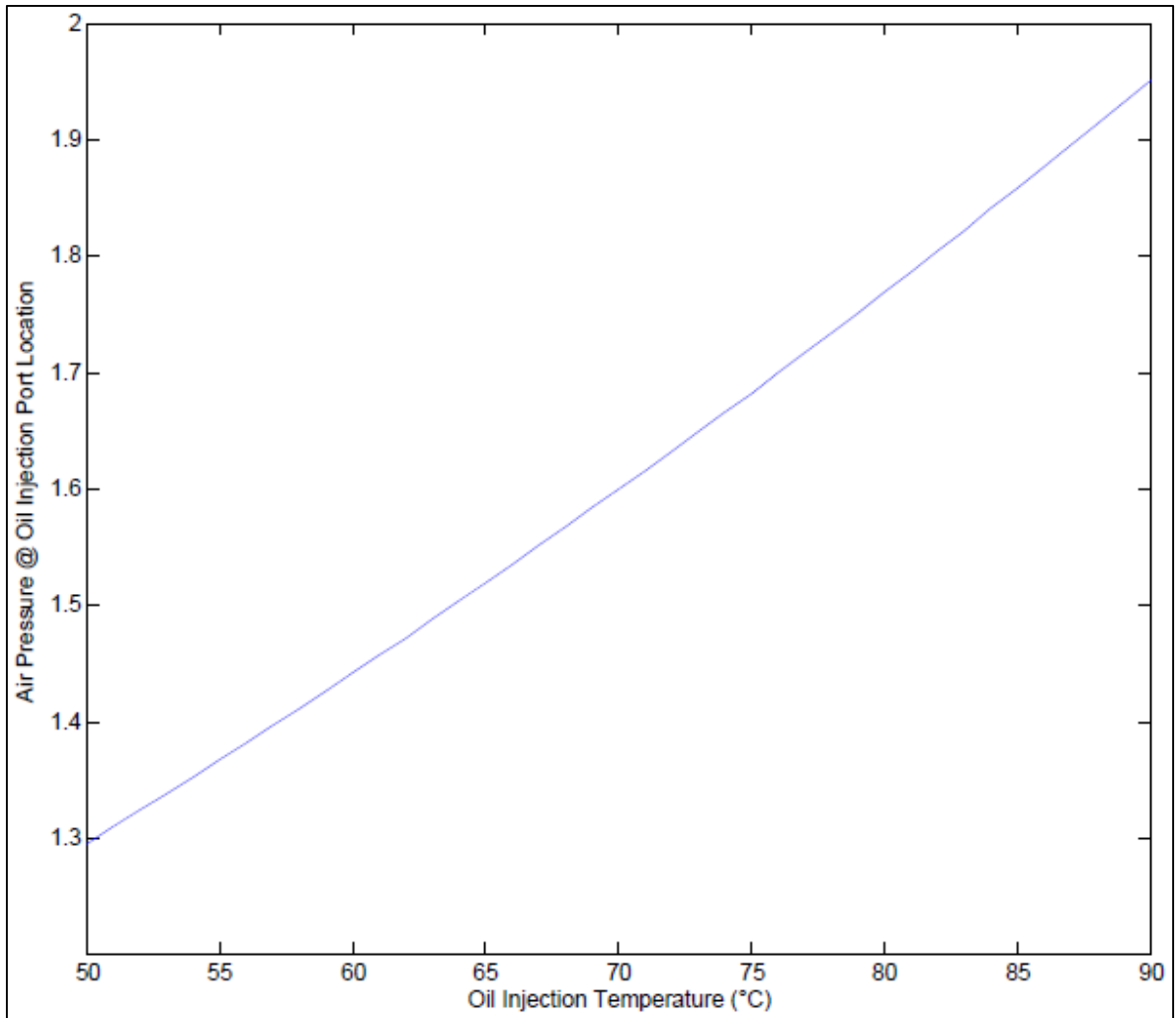


Figure 2.7. Results for oil injection temperature vs. air pressure in pressure chamber at oil injection port location

In order to calculate the oil injection port location, the pressure chamber of compressor has been modelled with Solidworks. Then, the chambers are observed according to the rotational position of rotors. While the rotors are turning, chamber starts to get smaller. The changes of volumetric ratio show ideal oil injection port location (Figure 2.8). The origin of coordinate system is on the beginning plane of the rotor profiles, which is shown in Figure 2.7.

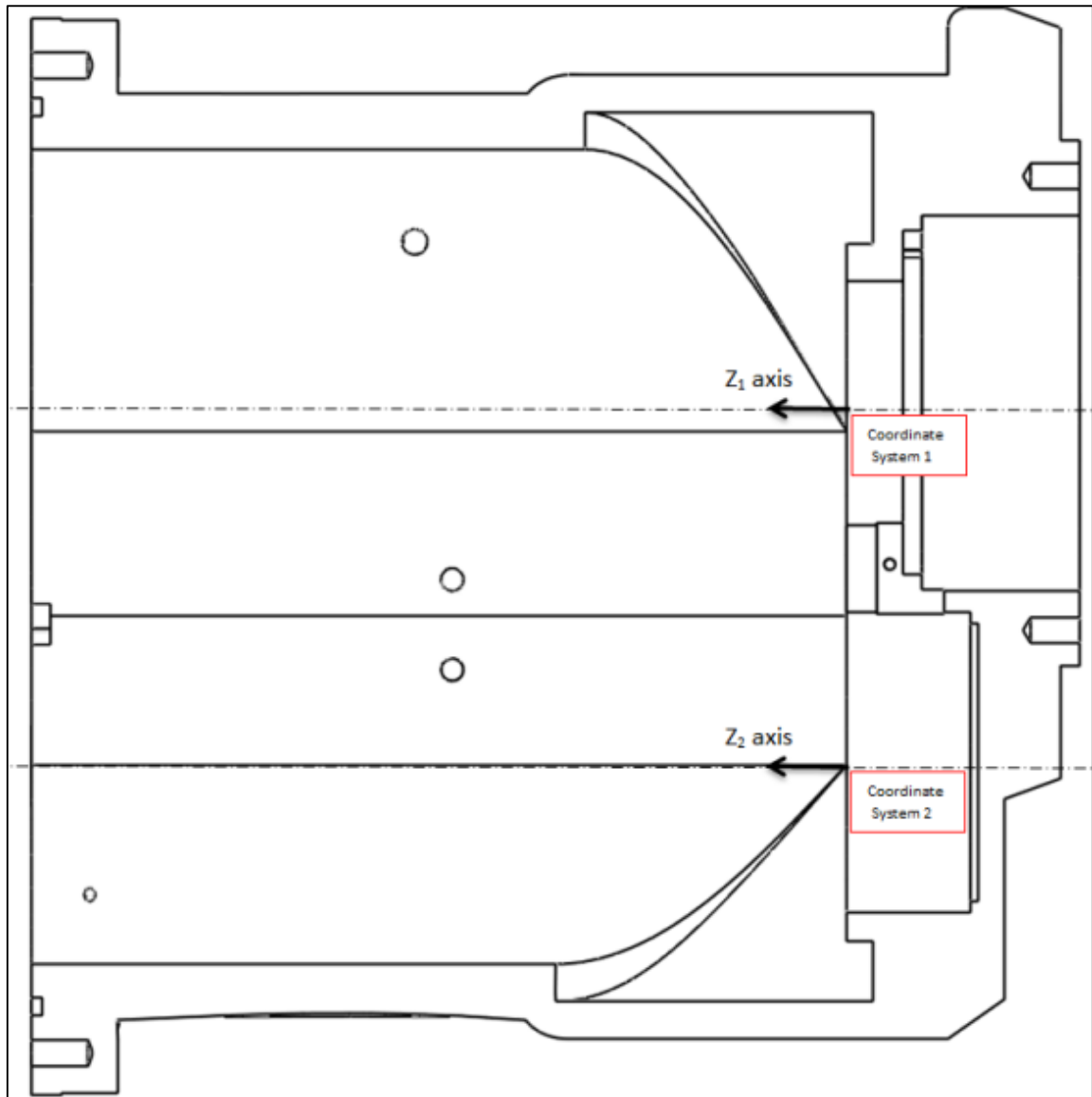


Figure 2.8. Coordinate System Z1 and Z2 axes

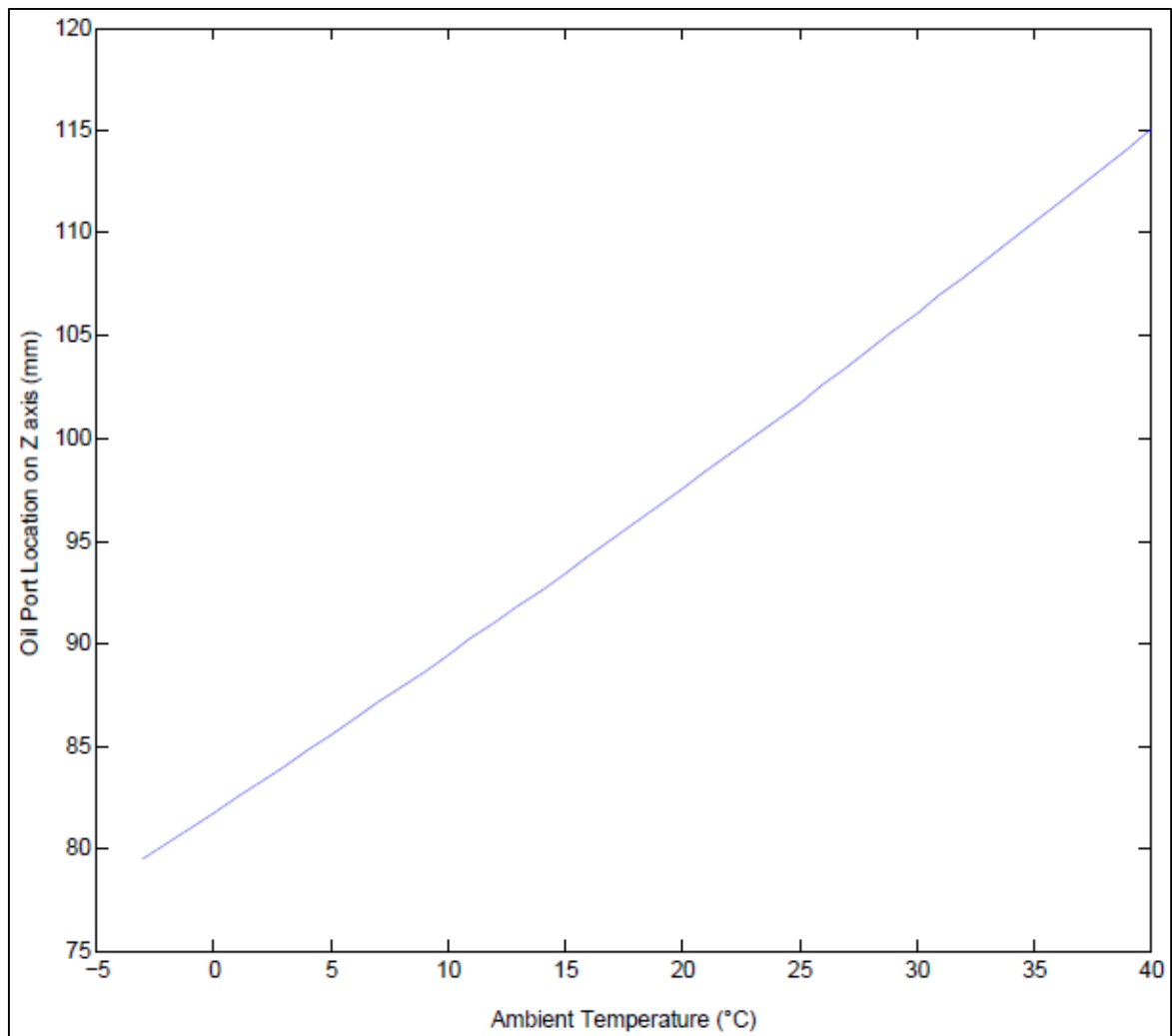


Figure 2.9. Results for ambient air temperature vs. oil port location on Z axis

Oil injection temperature may be most vital point for the compressor performance [47]. Although temperature can increase or decrease, oil injection ports cannot change their positions. The results for the change in oil injection temperature versus ambient temperature is in Figure 2.9.

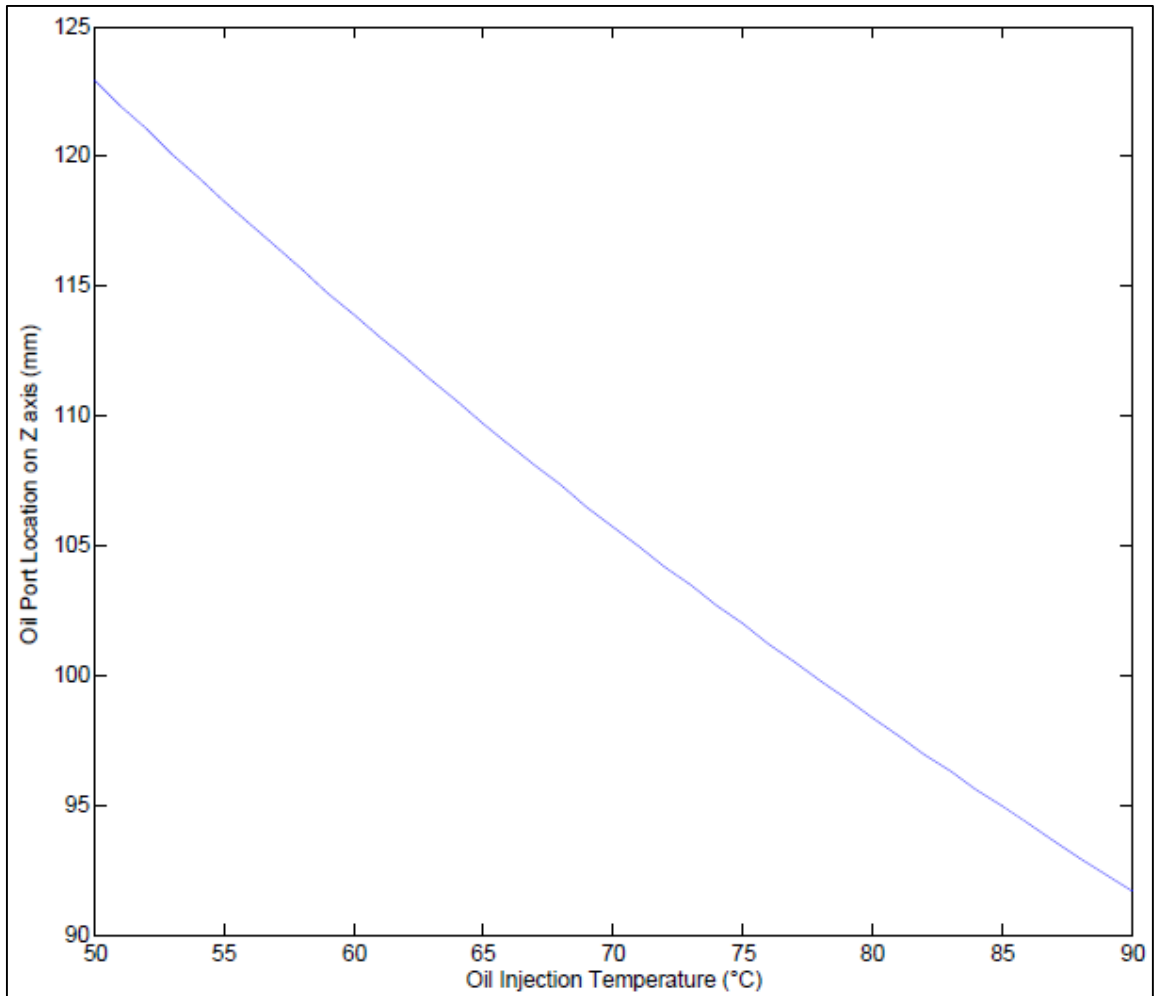


Figure 2.10. Results for oil injection temperature vs. oil port location on Z axis

To validate the theories, a commercial oil injected screw compressor unit is investigated in this section. The unit has 35 kW shaft power and 5 m³/min air flow capacity. First assumption of performed calculations is the ideal and complete heat transfer between air and oil droplets. In order to calculate the heat transfer efficiency simulations or experiments must be performed. Heat transfer efficiency calculation is the subject of another study. All leakages are ignored, because estimation of them is really difficult. Leakages result from a number of factors such as surface finishing of rotors and casing, pressure, temperature, rotational velocity of rotors etc. [48]. Rotor and casing heat transfer to the medium are ignored for simplicity purpose. Furthermore, isentropic compression is assumed; therefore, entropy values at the air suction and injection ports are identical.

Table 2.1. Air properties

Air @ Suction port :	
Temperature:	27°C
Pressure:	1 atm
Specific entropy:	1.7020 kJ/kg.K
Air @ Injection port:	
Temperature:	73°C
Pressure:	Calculated Below
Specific entropy:	1.8454 kJ/kg.K

$$s_2 = s_1 + R * \ln\left(\frac{P_2}{P_1}\right) \quad (2.5)$$

P_2 was calculated to be 1.648 bara and specific volume ratio was obtained to be 0.71. As a result of calculation with a specific heat rate, oil should be injected when the air pressure reaches to 1.648 bara. If the pressure chamber volume decreases to 71% of the initial volume, the air pressure reaches to 1.648 bara [49], [50], [51].

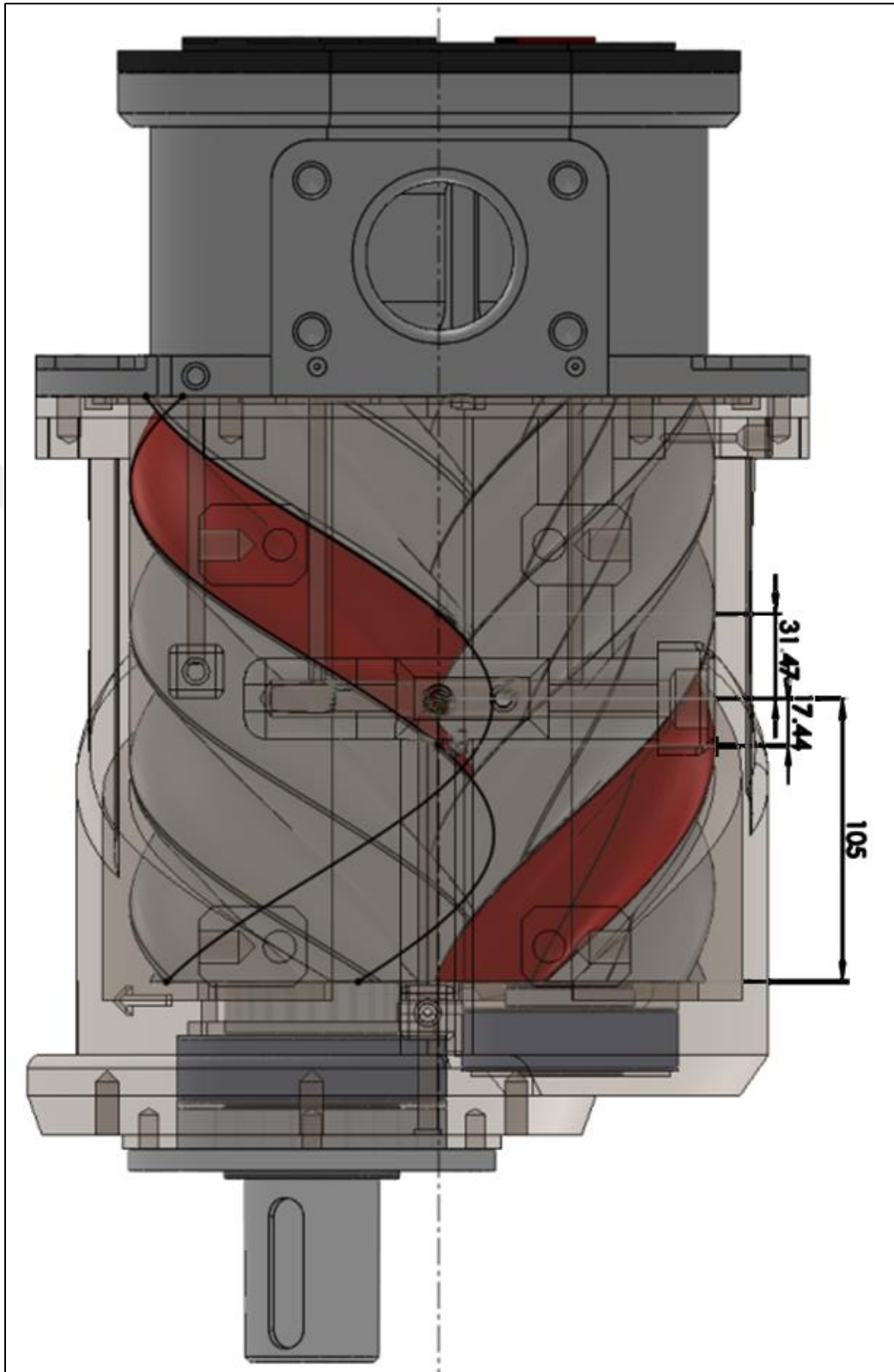


Figure 2.11. The estimated location of the oil injection ports on Z axis (Volumetric change of the pressure chamber was calculated with Solidworks.)

For 5 to 4 lobe screw compressors, a gear ratio 41.67/50 is assigned between female and male rotors. Each rotor has equal pressure chamber volume and the chambers are united. When the volume of the pressure chamber decreases to 1/3.3 (i.e. internal volume ratio) of the suction, the discharge port opens. This ratio is observed with a step by step modelling in a CAD software(Solidworks). Calculated range of the oil injection ports locations on z axis is between [105-17.44, 105+31.47] (mm) (Figure 2.10). If the suction air temperature is lower, overall performance of a compressor increases in general. Low temperature means low moisture in air and high density in pressure chamber, so the mass of the sucked air increases. If the oil cooler performance with respect to ambient air temperature is ignored, cooling air performance in the pressure chamber decreases proportional to temperature. As the air temperature in the pressure chamber cannot reach to oil injection temperature at the injection point, the oil injection ports get closer to the discharge port and decreases the duration of oil particles in the pressure chamber. Therefore, cooling cannot be performed efficiently. The oil injection port location versus ambient temperature graph (see Figure 2.9) shows how the oil injection ports change their location according to the ambient temperature.

The results show that the calculated locations of the oil injected port are very close to those of commercial screw compressor unit with a 3% error percentage in z axis. Besides, oil injection flow rate is 11% greater than commercial air end, because overflow causes oil stack between rotor couples or between rotors and casing. The overflow can only be observed with experiments, the air end producer has to decrease theoretical oil injection flow rate.

2.2. OIL VOLUMETRIC FLOW RATE FROM OIL INJECTION NOZZLE

Another problematic point is how much oil must be injected to the pressure chamber. Over injection causes stuck rotors as a result of high oil quantity in chamber. On the other hand, in case there is not enough injection, oil in the compressor system gets burned [52], [53]. Because the air temperature become higher than the flash point of oil before oil particles leave the pressure chamber. Oil burning is a chain reaction that's why all the oil burns inside the compressor system. For cleaning this oil, two times of compressor oil in reservoir must be consumed. Oil injection flow rate depends on the oil injection temperature and air flow rate.

Theoretically increments in oil flow rate increases dissipated heat flow rate air to oil [54]. Although theoretical compressor efficiency is increased, due to the oil stack between rotors the overflow of oil injection decreases efficiency. Figure 2.12 shows the required oil injection flow versus discharge air temperature in ideal conditions. In equation 2.6 \dot{m}_1 represents mass flow air on suction port of air end, and h_1 is the enthalpy of the ambient air. \dot{m}_2 is the injected oil mass flow rate, and h_2 is enthalpy of injected oil. Enthalpies of the discharged air and oil are h_3 and h_4 , respectively.

$$\dot{m}_1 h_1 + \dot{m}_2 h_2 = \dot{m}_1 h_3 + \dot{m}_2 h_4 \quad (2.6)$$

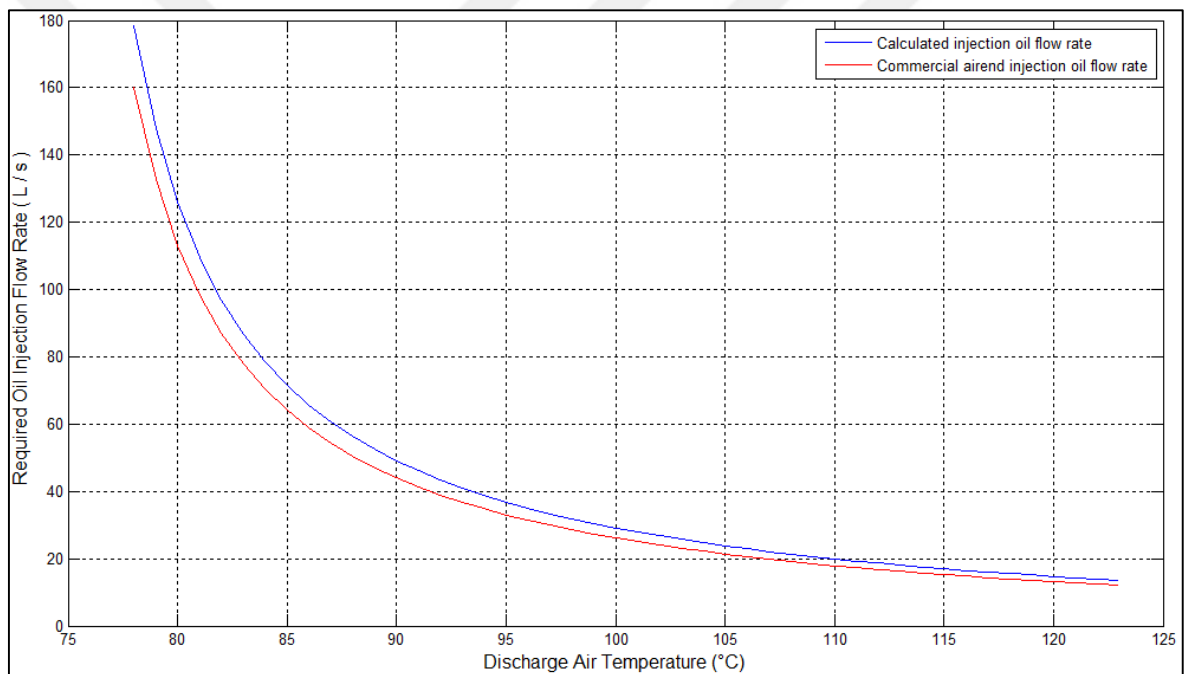


Figure 2.12. Mathematical and Analytical results and experimental observation of required oil injection flow rate vs. discharge air temperature

As a result of ideal heat transfer assumption, oil injection temperature and discharge air temperature are linearly proportional dependents. The oil injection flow rate calculated with the equation 2.6 is shown with a blue curve and oil injection flow rate of commercial aircend is drawn with a red curve on Figure 2.12.

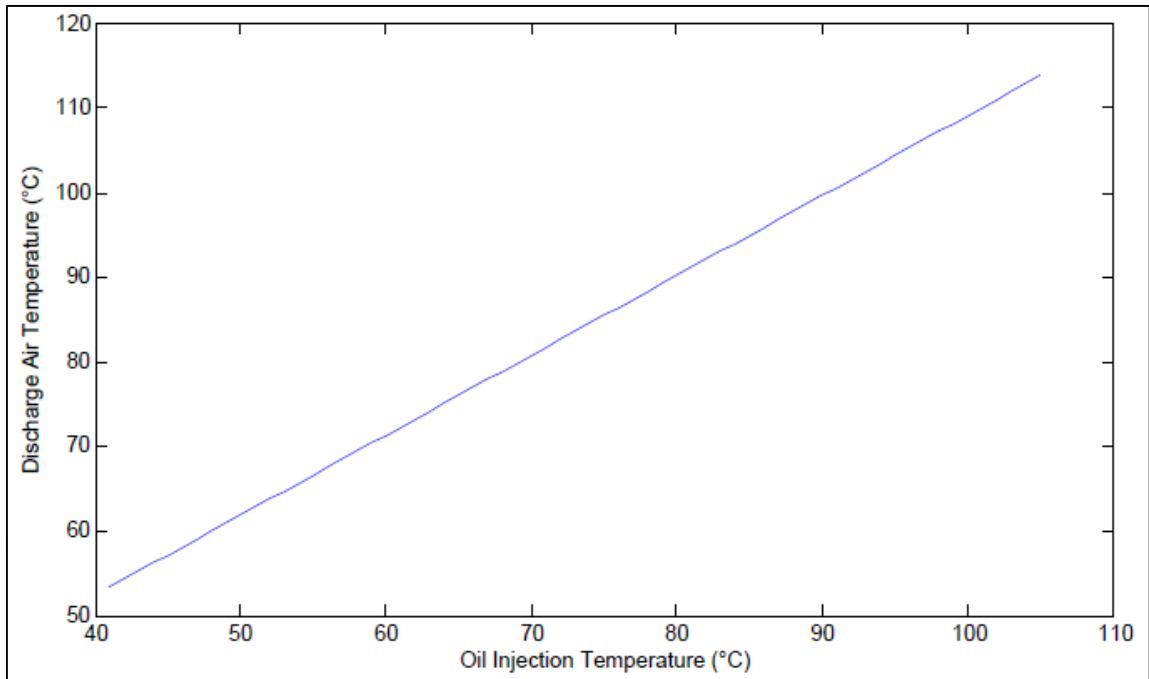


Figure 2.13. Results for discharge Air Temperature vs. Oil Injection Temperature

While oil particles in air medium flow through the discharge port, temperature difference between the oil particles and pressurized air decreases, and the heat transfer efficiency decreases as well. The assumption about the perfect heat transfer requires ignoring the heat transfer efficiency.

It is evaluated that how much oil injection a compressor with $5 \text{ Nm}^3/\text{min}$ air suction capacity needs in order to cool discharged air to 80°C . (Figure 2.13). At first, the calculations are made about what air temperature would be if there was no coolant injection, Assumption of calculations is the ideal and complete heat transfer between air and oil droplets. Because in order to calculate heat transfer efficiency, some simulations or experiments must be performed and they are the subject of another study. All leakages are ignored. Estimation of leakages is very difficult. Leakages depend on a lot of factors; such as finishing of rotors and casing, pressure, temperature, rotational velocity of rotors etc. [55], [56] Rotor and casing heat transfer with the medium are ignored with the aim of simplicity. Furthermore, isentropic compression is assumed; therefore, entropy values at the air suction and injection ports are identical. Entropy function is defined as follows:

$$s^o = \int_0^T c_p(T) \frac{dT}{T} \quad (2.7)$$

Table 2.2. Air properties for oil injection temperature calculation

Air @ Suction port :		
	Temperature:	27°C
	Pressure:	1 atm
	Specific entropy:	1.7020 kJ/kg.K
Air @ Discharge port:		
	Temperature:	Calculated below
	Pressure:	7 barg
	Specific entropy:	Calculated below

$$s_2 = s_1 + R * \ln \frac{P_2}{P_1} \quad (2.8)$$

Entropy at state 2 is calculated to be 2.2988 kJ /kg. K and temperature is 267 °C. The discharged air (@7barg) temperature is 267°C without coolant injection. Target value of the oil injection temperature is 73°C which is the opening port temperature of the thermostatic valves commonly preferred by most of the companies. Colder injection (lower limit is about 60°C) certainly improves performance.

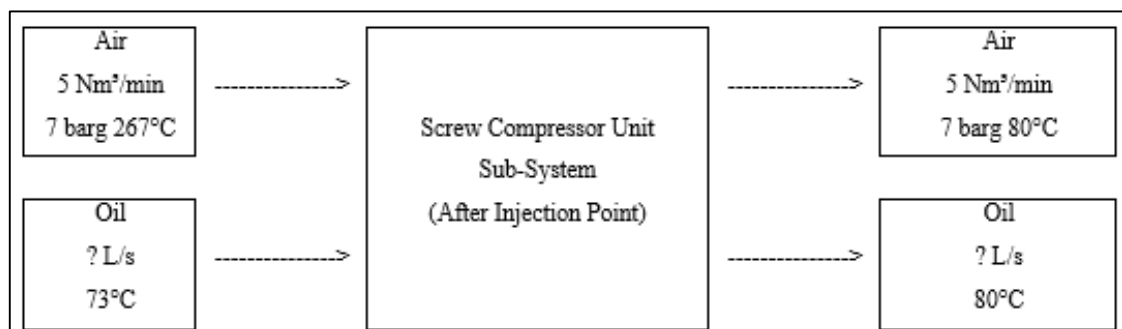


Figure 2.14. Thermodynamic schematic of standard cooling system of air end

$$\dot{m}_1 h_1 + \dot{m}_2 h_2 = \dot{m}_1 h_3 + \dot{m}_2 h_4 \quad (2.9)$$

$$\dot{m}_2 = 108.11 \text{ kg/min}$$

Table 2.3. Air properties for oil injection flow rate calculation

Oil specification @ Injection port:		
	Temperature:	73°C
	Density:	858 kg/m ³
	$\dot{v}_2 = 126$ L/min	
Test results:		
	Air flow rate:	5 Nm ³ /min
	Oil flow rate:	113 L/min

As a result of these calculations; oil flow rate theoretically should be 126 l/min in order to cool the discharge temperature to 80°C. The commercial air end (EVO9) from Rotorcomp Company needs 113 l/min oil injection to pressurize 5 Nm³/min air at 1 atm up to 7 barg. The difference stems from gear design. If gearbox is exposed to over injection of oil, gears can be stuck or turn harder than they need to do. It is normal to evaluate a higher oil flow rate with theoretical calculation. Because theoretical calculation shows only the initial point of oil injection flow rate for trying on air end. The remaining approach to find optimum point must be performed by experiments by trial and error.

2.3. OIL INJECTION NOZZLE DIAMETER

Besides the importance of oil injection quantity, dimensions of oil particles in the air are also important for the cooling performance. If the particle is too small, it cannot resist centrifugal force and sticks to the outer walls of chamber. On the contrary, if the particle diameter is too small, it is not affected by the centrifugal force, so it directly sticks to the surface of rotors. Moreover, surface areas are smaller in larger particles than small particles. The optimum diameter for the most efficient heat transfer has been examined and formulated with studies [40].

A flying droplet in a medium may break up, the occurrence of the breakup and the new diameters of oil droplets are dependent to Weber number. For weber value, medium and particle speed are important parameters. Oil injection nozzle outlet section assumed as flat although it has a curved shape due to the chamber of rotors. Sparse oil droplets are assumed, in other words, there is no interaction between droplets. Oil viscosity is constant in all calculations, because the injection point is important for calculations and the time so short

that there is no change in oil temperature. Oil droplets are always assumed to have spherical geometry with no deformation. Weber number (Eq. 2.6) is especially used to estimate the collision or breakup of particles.

$$We = \frac{\rho_p v^2 l_p}{\sigma_p} \quad (2.10)$$

ρ_p represents the particle density in this calculation and particle density is equal to the oil density. v is the particle's swimming velocity in air medium. v equals to (Oil volumetric flow / Injection port area). l_p is characteristic length which can be assumed to be equal to d_0 injection port diameter. σ_p is the tension of particle surface, it determines the oil particle's surface to friction while swimming in the medium. Oil surface tension is 0.0320 N/m according to the referenced article [57].

$$\rho_p = 858 \text{ kg/m}^3$$

$$v = \frac{2.1 \cdot 10^{-3} [m^3/s]}{(\pi d_0^2 / 4)}$$

Table 2.4. Table of oil injection particle and nozzle properties

Assumption:	$l_p = d_0$	[40]
Surface tension of oil droplet:	$l_p = 0.0320 \text{ N/m}$	[41]
After some evaluations;		
For single oil injection port:	$We = 0.1917/d_0^3$	Eq.2.6
For double oil injection port:	$We = 0.04792/d_0^3$	Eq.2.7

After the Weber number is calculated, the formula by Isshiki (1959) [40] can be evaluated. The formulation made by Isshiki is a non-linear differential equation, so non-linear solver software is used for evaluation [40].

$$\left(\frac{d}{d_0}\right)^{0.25} = \frac{1.9}{W_0^{0.25}} + 0.315 \left(\frac{\rho_g}{\rho_p}\right)^{1.5} C_{D_0} W_0^{0.125} \ln\left(\frac{d}{d_0}\right) \quad (2.11)$$

Table 2.5. Table of oil particle properties for nozzle diameter calculation

CDo= 1 (Drag coefficient of oil droplet is assumed as 1 according to Singh et. al(1986)[57])	
d = 1000 nm (The maximum efficiency for particle diameters 1000 nm Singh at.al(1986)[57])	
ρ_g = density of medium at the injection pressure of pressure chamber (Air@1.68 bara =>1.59 kg/m ³)	
$d_0 = \text{orifice diameter (Nozzle Diameter)}$	Assumption [40]
$C_{D_0} = 1$	Assumption [40]
$d = 1000 \text{ nm}$	Particle Diameter [40]

$$\left(\frac{1000 \cdot 10^{-9}}{d_0}\right)^{0.25} = \frac{1.9}{W_0^{0.25}} + 0.315 \left(\frac{1.59}{859}\right)^{1.5} \cdot 1 \cdot W_0^{0.125} \cdot \ln\left(\frac{1000 \cdot 10^{-9}}{d_0}\right) \quad (2.12)$$

Non-Linear Equation (Evaluated by MATLAB solver)

Table 2.6. Result list of oil injection nozzle diameter calculation

For single oil injection port:	$We = 0.1917/d_0^3$
	$d_0 = 11 \text{ mm}$
For double oil injection port:	$We = 0.04792/d_0^3$
	$d_0 = 7.8 \text{ mm}$
Calculated port cross-section area:	$A_{port} = 47.784 \text{ mm}^2$

As a result, the oil injection port diameter was calculated as 11 mm for one oil injection nozzle and 7.8 mm for two oil injection nozzles. Because of the curved surface of casing, a hole drilled with 6.5 mm diameter provides the calculated area with 46.286 mm². (Figure 2.14) (The exact value is 47.784 mm², but the difference between the exact and calculated values is acceptable.)

If the equation is performed for a different flow rate, it can be observed that the increments in the injection hole diameter are getting slower.

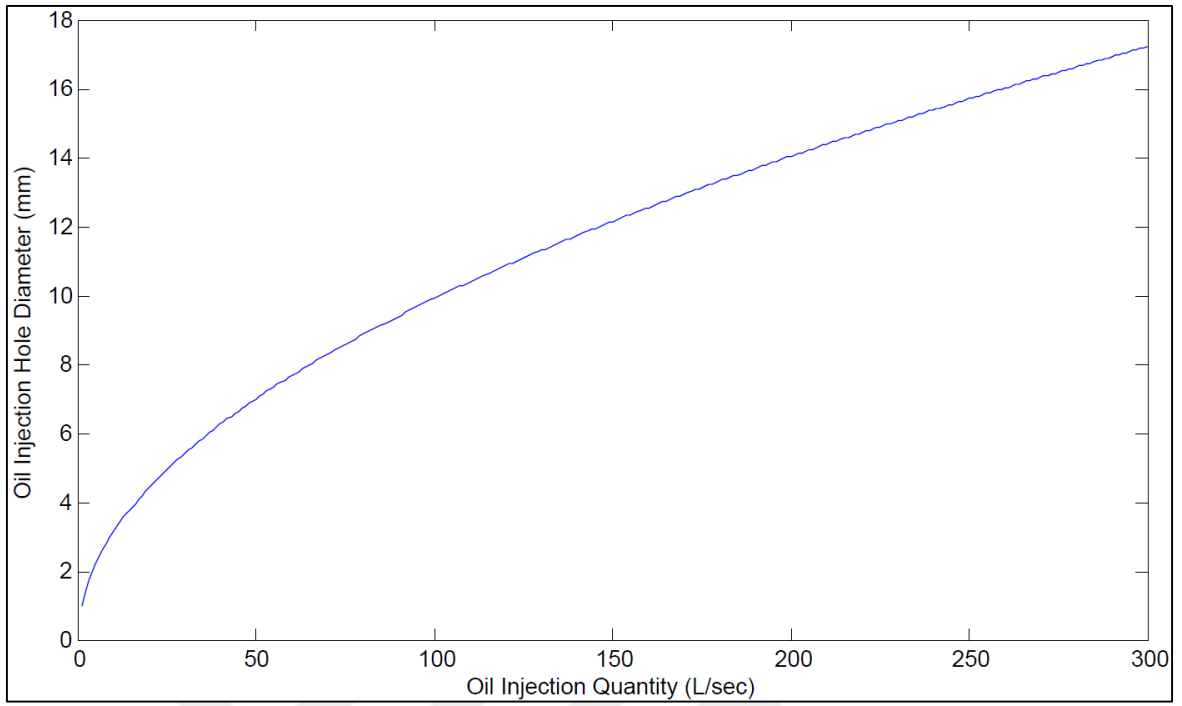


Figure 2.15. Results for oil injection hole diameter vs oil injection flow rate

3. INLET DIAMETER AND FLOW VOLUME EFFECTS ON THE SEPARATION AND ENERGY EFFICIENCY OF HYDROCYCLONES

3.1. NUMERICAL MODEL

In industry, one of the methods for compressing air is to use oil injected screw compressors. In this type of compression, oil is injected into air end to ensure lubrication of the rotating screws and to provide sealing for air leakage (i.e., preventing back flow of air). Once the compression is performed, oil and air mixture needs to be sent to the hydrocyclones where air is separated from oil. In this study, a simplified numerical model is generated to study the performance of separation and energy efficiencies of the hydrocyclones. This model was also described and used by Xiang Gao [58] to investigate the effects of the central channel on the flow field in an oil-gas hydrocyclone. In this study, three dimensional hydrocyclone model with rectangular inlet was investigated and is shown in Figure 3.1. The diameter of main body is lettered by D and all simulation has been performed considering D is equal to 0.65 m. Parameters to describe the hydrocyclone are given in Table 3.1.

Table 3.1. Hydrocyclone geometric parameters

Swirl volume height	(H)	2D			2.5D			3D		
Inlet duct height	(a/D)	0.3	0.4	0.5	0.3	0.4	0.5	0.3	0.4	0.5
Inlet duct width	(b/D)	0.15	0.1 5	0.15	0.15	0.1 5	0.15	0.15	0.1 5	0.15
Inlet duct area	$((a*b)/D^2)$	0.04 5	0.0 6	0.07 5	0.04 5	0.0 6	0.07 5	0.04 5	0.0 6	0.07 5
Central duct diameter	(d)	0.5D			0.5D			0.5D		
Central duct height	(h)	D			D			D		
Central duct inlet length	(L)	D			D			D		
Diameter	(D)	D			D			D		

The numerical model illustrated in Figure 3.1 was generated with SolidWorks based on the parameters provided in Table 3.1. Three-dimensional hydrocyclone geometry was imported to ICEM-CFD for meshing (Figure 3.2). The number of elements was different for each simulated case, because the geometry was changing from one case to another. Table 3.3 below provides the mesh information of the studied nine different cases. In these models, grid independency is ensured by Xiang Gao in his article [58]. For these nine cases, grid independency is checked again with a geometry of “H=3D” and “a=0.5D”, and inlet velocity is assumed to be equal to 17.33 m/s at 0.2 MPa. The simulation results are shown in Table 3.2. Briefly, three different swirl volume height (H = 2D, 2.5D, and 3D), with three different hydrocyclone inlet duct sizes (0.15D x 0.3D, 0.15D x 0.4D and 0.15D x 0.5D) were used to study the effects of the separation and energy efficiency of hydrocyclones. In order to observe the effects of the inlet diameter and swirl volume height on hydrocyclone performance, nine different combinations of diameter and height sets were created and listed in Table 3.3. Figure 3.2 shows the computational grid of the numerical model for swirl volume height which is 3D and the height of hydrocyclone inlet duct which is 0.5. Simulation was performed with three different number of meshes. The difference of pressure losses of simulations in acceptable range is about 0.2%. Total number of elements are 258,064.

Table 3.2. Grid independency check results for 3D main body diameter and 0.5D inlet duct height case

Grid Independency Check Results	
Number of cells	Total pressure loss of oil tank(Pa)
175002	2842
238938	2830
308442	2835
Difference between finest and coarsest mesh (%)	0.2%

Table 3.3. Studied cases (total of nine different models was generated for the study)

Swirl volume height (H)	2D			2.5D			3D		
Height of inlet duct (a/D)	0.3	0.4	0.5	0.3	0.4	0.5	0.3	0.4	0.5
Number of Cells	203269	206473	203353	226227	229088	245907	255255	257837	258064

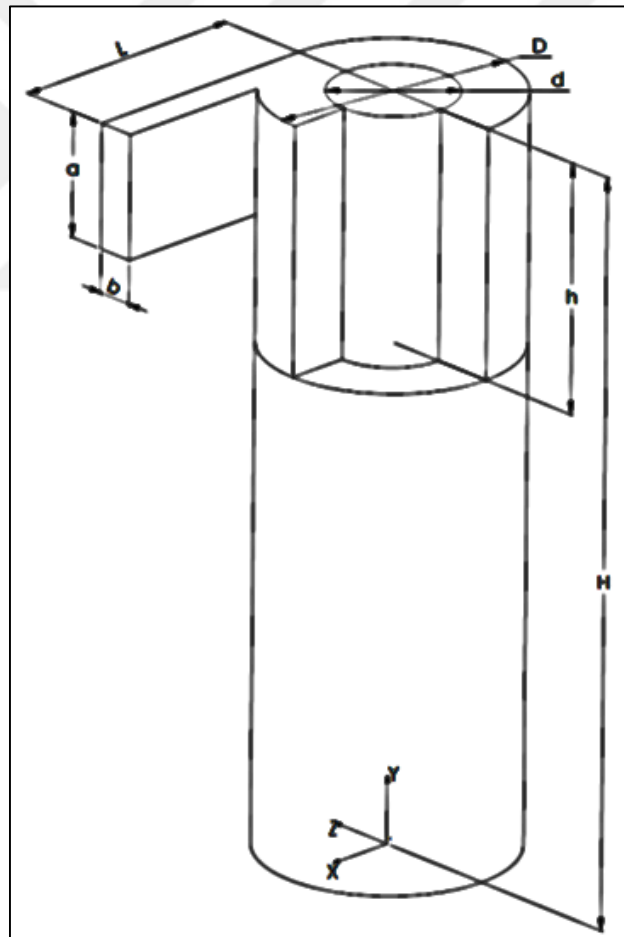


Figure 3.1. Numerical model with parameters

Once the meshing was completed, boundary conditions could be defined. Pressure and velocity were coupled in the equations of motion for incompressible flows. As an outlet boundary condition, a static pressure value of pressure outlet was specified while velocity inlet boundary condition was assigned for the inlet. Thus, the velocity at the outlet surface must adjust itself to match the rest of the flow field, similarly at the inlet surface the pressure needs to adjust itself so that the inlet and outlet boundary conditions were not over specified mathematically. DPM particle injection surface was also employed to the inlet surface. In DPM modeling settings, inlet and outlet surfaces were assumed to be escape boundary condition. All the walls were modeled with no slip boundary wall condition except for the bottom wall. The bottom wall was set to no slip boundary wall condition for turbulence model and trap model for DPM model. Gravity was also defined along -y direction for all simulations. Material properties of air and oil were defined for computational grid. Specifically, the air density and viscosity were taken as 3.5 kg/m^3 and $2.09 \times 10^{-6} \text{ kg/m.s}$ at 0.2 MPa, respectively. Pressure and the oil density and viscosity were taken as 830 kg/m^3 and 5.08 kg/m.s at 95°C , respectively.

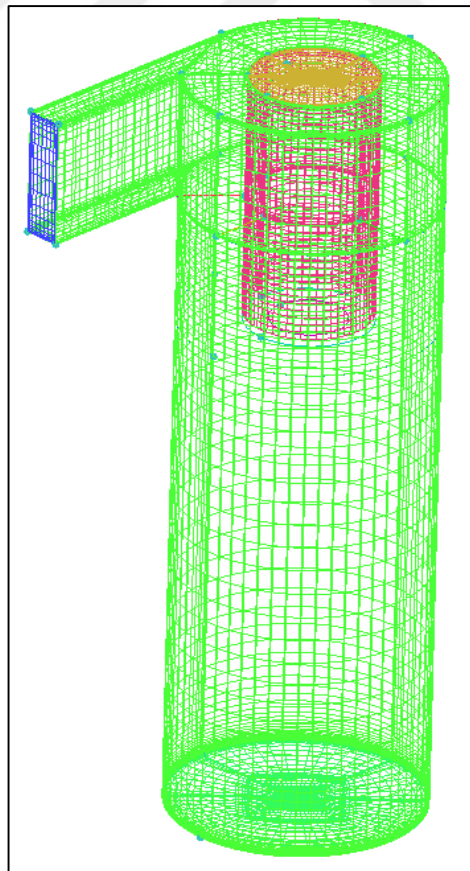


Figure 3.2. Numerical model with computational grid

Mainly three assumptions were made during this study. First assumption was about the inlet of the cyclone. In this study, a rectangular duct was used instead of a circular pipe. Second assumption was regarding to the oil reservoir. The oil reservoir below the tank was assumed to be a wall with trap condition so that oil surface flow of oil reservoir remained the same. Therefore, the bubble and the returning cached particles would be eliminated. Third assumption was about the shape of the particles. The particles in the study were proposed to be a spherical ball and no change in their shape was allowed during simulations.

In the numerical model, the RSM is preferred for the viscous turbulence model. For tracing droplets, DPM model was used with sub modules like Saffman Lift force, Discrete Random Walk (DRW), Breakup, Stochastic Collision and Coalescence. There are a lot of combinations of turbulence solver models for the solution of different flow problems moderately or for decreasing computational time in Fluent. Kaya and Karagöz [30] discuss the best combination for solver models. The most convenient combination were found to be PRESTO for pressure discretization, SIMPLEC for pressure velocity coupling, QUICK for momentum discretization, second-order upwind for turbulent kinetic energy and turbulent dissipation rate and lastly first order upwind for Reynolds stress based on their study. In turbulence modelling, the Reynolds Stress Model (RSM) was utilized to solve Reynolds-averaged Navier-Stokes equations. Although the use of RSM increases the computation time of the simulation, this model is typically recommended for cyclones, highly swirling flows in combustors, rotating flow passages, and the stress-induced secondary flows in ducts. Discrete phase model (DPM), utilized in this study, is widely used for the particle flows. In this model, particles were added to the flow to track the liquid droplets. The volume fraction of oil particles was generally lower than 10-12% in the flow, so they did not influence the main phase flow inside the oil tank. The velocity of the particle was dependent on shear force in the particle, main phase velocity and the particle itself.[59] Another additional parameter was related to velocity of particle which is particle acceleration “a” due to other forces on the particle.

$$\frac{du_p}{dt} = \frac{1}{\tau_p} (u - u_p) + a \quad (3.1)$$

After some analytical integration, the particle velocity at new location n+1 was formulated as:

$$\mathbf{u}_p^{n+1} = \frac{\mathbf{u}_p^n + \Delta t \left(\mathbf{a} + \frac{\mathbf{u}_p^n}{\tau_p} \right)}{1 + \frac{\Delta t}{\tau_p}} \quad (3.2)$$

And the new location was computed with basic location formula of physics.

$$\mathbf{x}_p^{n+1} = \mathbf{x}_p^n + \frac{1}{2} \Delta t (\mathbf{u}_p^n + \mathbf{u}_p^{n+1}) \quad (3.3)$$

Forces acting on a particle defining the acceleration of that particle were formulated with Lagrangian model in Fluent. The acceleration of a particle was essentially determined by the drag force, density difference between the main flow and particle, and also an additional acceleration force symbolized as F_x . This force played an important role when the density of the main phase was greater than the density of the particle.

$$\frac{d\mathbf{u}_p}{dt} = F_D (\mathbf{u} - \mathbf{u}_p) + \frac{g_x (\rho_p - \rho)}{\rho_p} + F_x \quad (3.4)$$

$$F_D = \frac{18\mu}{\rho_p d_p^2} \frac{C_D \text{Re}}{24} \quad (3.5)$$

$$\text{Re} \equiv \frac{\rho d_p |\mathbf{u}_p - \mathbf{u}|}{\mu} \quad (3.6)$$

Re symbolizes Reynolds number. The oil particles have greater density than air; therefore, F_x becomes negligible. The Saffman's lift constant is greater than other additional acceleration force terms, so only Saffman's lift force was considered in current study.

$$\vec{F}_x = \vec{F} = \frac{2Kv^{1/2}pd_{ij}}{\rho_p d_p (d_{lk}d_{kl})^{1/4}} (\vec{u} - \vec{u}_p) \quad (3.7)$$

Instantaneous oil droplet velocity was included to observe that particles in the turbulent flow when DRW model was activated. The DRW model, uses the fluctuating velocity components, is a discrete piecewise constant functions of time:

$$\mathbf{u} = \bar{\mathbf{u}} + \mathbf{u}' \quad (3.8)$$

As a result of particle collisions, the particle diameter increases. When the particle diameter and its velocity reach to a certain value, the particle may break up into tinier particles before it is collided again. The collision possibility of a particle with N-1 particles is approximately $(1/2) N^2$. When two particles collide, they may be coalesced or bounced. The reaction of the collision of two particles can be calculated by a collisional Weber number.

$$We_c = \frac{\rho U_{rel}^2 \bar{D}}{\sigma} \quad (3.9)$$

When two particles collided, the event results in coalescence or elastic collision. There is also another type of coalescence: if the two particle flow to the same direction and get closer to each other below the critical distance, they coalescence. The critical offset depends on the Weber number and the relative radius between particles. The critical offset has been formulated by O'Rourke [60] and is given as:

$$b_{crit} = (r_1 + r_2) \sqrt{\min(1.0, \frac{2.4f}{We})} \quad (3.10)$$

The actual collision parameter b equals to $(r_1 + r_2)\sqrt{Y}$. Here, Y is a random number between 0 and 1. If the b_{crit} is greater than the actual b , particles are collided resulting in coalescence. The term f is related the ratio between particle radius.

$$f\left(\frac{r_1}{r_2}\right) = \left(\frac{r_1}{r_2}\right)^3 - 2.4\left(\frac{r_1}{r_2}\right)^2 + 2.7\left(\frac{r_1}{r_2}\right) \quad (3.11)$$

O'Rourke [60] claims that the coalescence causes energy loss; therefore, the coalescent particle velocity cannot be calculated since momentum equation would not be enough. The derived expression for the coalescent particle velocity can be computed from:

$$V_1' = \frac{m_1 v_1 + m_2 v_2 + m_2 (v_1 + v_2)}{m_1 + m_2} \left(\frac{b - b_{crit}}{r_1 + r_2 - b_{crit}} \right) \quad (3.12)$$

In oil droplet breakup, Taylor analogy method is used for low-Weber-number injections. As a result weber number less than 100 the TAB model can be applicable. If one of the particle distortions equals the half of the droplet diameter, droplet is assumed to be broken up. The breakup occurs when y gets higher than 1 and y can be calculated with formula below.

$$y(t) = We_c + e^{-(t/t_d)} \left[(y_0 - We_c) \cos(\omega t) + \frac{1}{\omega} \left(\frac{dy_0}{dt} + \frac{y_0 - We_c}{t_d} \right) \sin(\omega t) \right] \quad (3.13)$$

3.2. VALIDATION OF NUMERICAL MODEL OF OIL SEPARATION TANK

The article by Xiang Gao [24] discusses their simulation and experimental results, so the results of the simulation can be compared with the experimental results. The deviation among the current study, experimental and simulation results by Gao's team is in acceptable level. The results provided in Table 3.4 are also plotted in Figure 3.3. For the flow with 14.4 m/s velocity the Low-Re Corrections option is enabled. There is deviation of an unacceptable level in the 15.20 m/s velocity row, and there are two reasons for this high deviation. Firstly, due to the low inlet velocity, some small vortices are observed near the inlet port. The other

reason is that when inlet velocity is equal to 15.20 m/s, Reynolds number is at the limit of Low-Re correction.

Table 3.4. Pressure loss variations with inlet velocity for Gao's experimental and numerical studies and current study

Inlet Velocity (in m/s)	18.10	17.29	16.89	16.30	15.20	14.40
Pressure drop comparison (in Pa)						
Experimental results	4495.3	3711.46	2808.99	2235.87	1861.66	1468.11
Simulation results by Xiang	4299.10	3487.84	2534.73	1913.09	1473.48	1320.43
Simulation results of current study	4239	3382	2645	2144	1529	1510
Deviations in simulation results						
Simulation results by Xiang	4%	6%	10%	14%	21%	10%
Simulation results of current study	6%	9%	6%	4%	18%	-3%

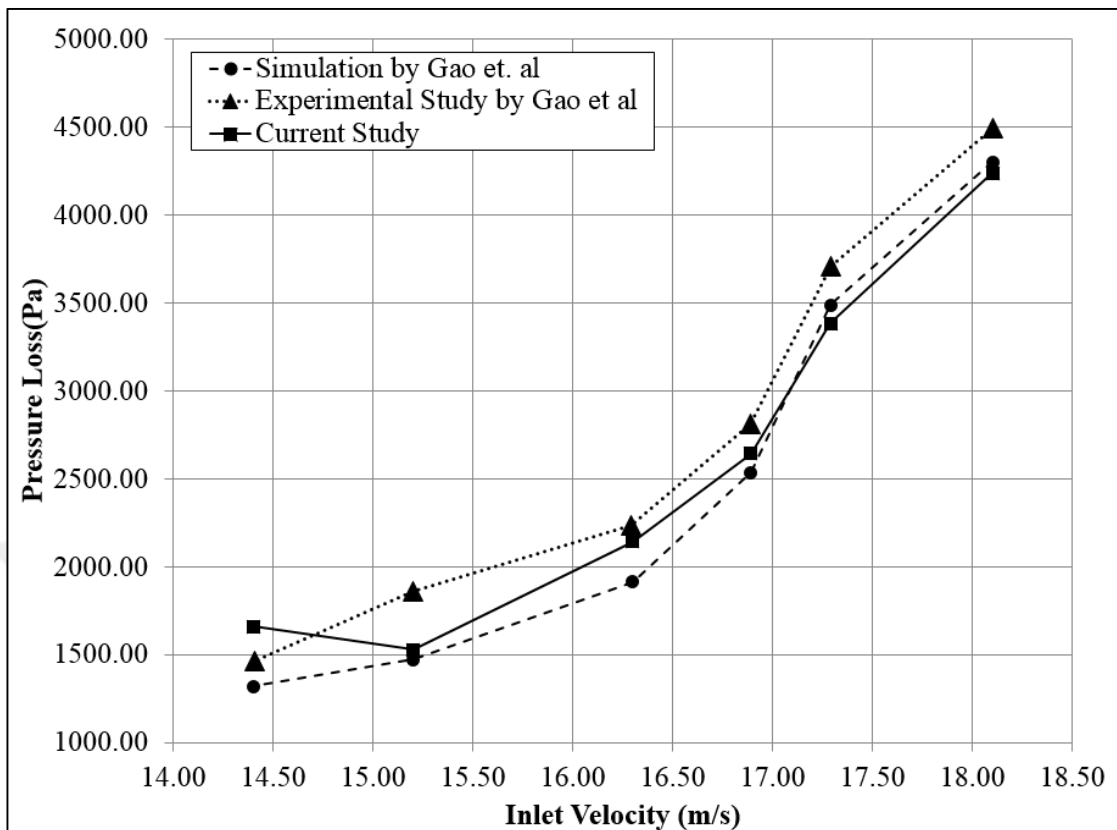
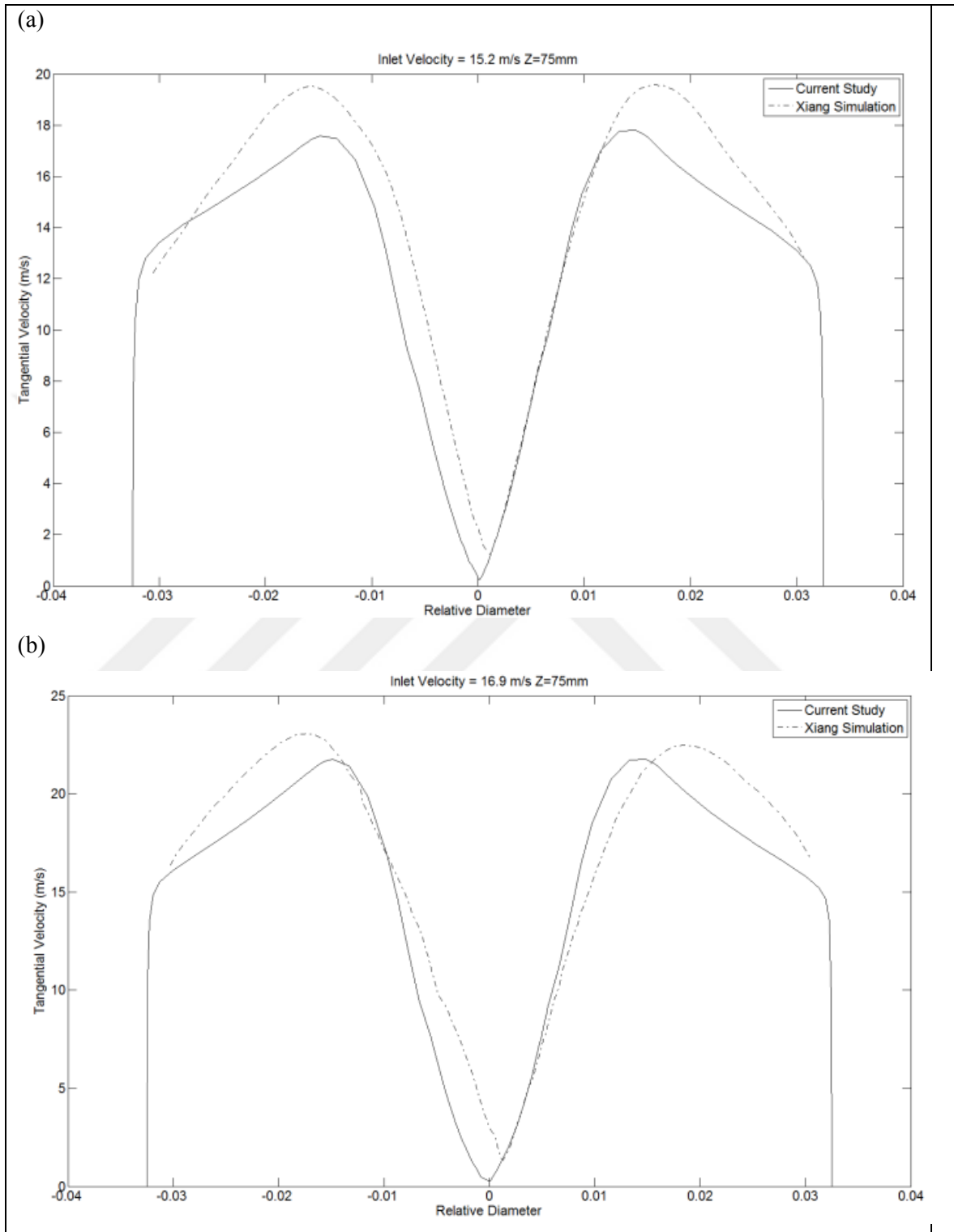


Figure 3.3. Pressure loss variations with inlet velocity for Gao's experimental and numerical studies and current study

Tangential velocities on the line parallel to the Z axis at the 75mm offset from the bottom surface are illustrated in Figure 3.4 which show us the central reverse flow swirl channel shape. Besides, tangential velocities are compared with the simulation results by Xiang Gao. [24] It is observed that difference is in acceptable range.



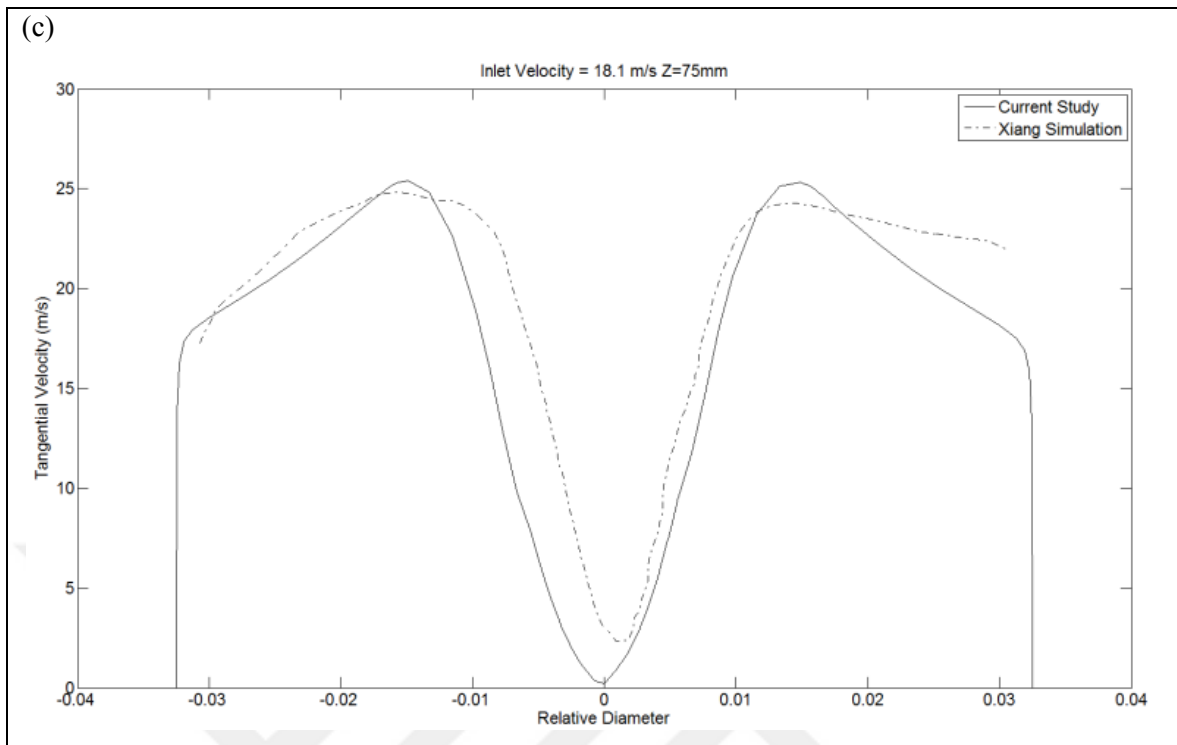


Figure 3.4. Tangential velocities on the line parallel to the Z axis at the 75 mm offset from $y = 0$ (a) at inlet velocity of 15.2 m/s (b) at inlet velocity of 16.9 m/s (c) at inlet velocity of 18.1 m/s

As a result of high swirl flow velocity, the cyclone with the lowest height has the highest pressure loss as shown in Figure 3.5. Furthermore, for the same volumetric flow rate while inlet diameter is decreasing, flow speed increases, therefore it is obvious that the pressure loss increases inversely in proportion to the inlet diameter.

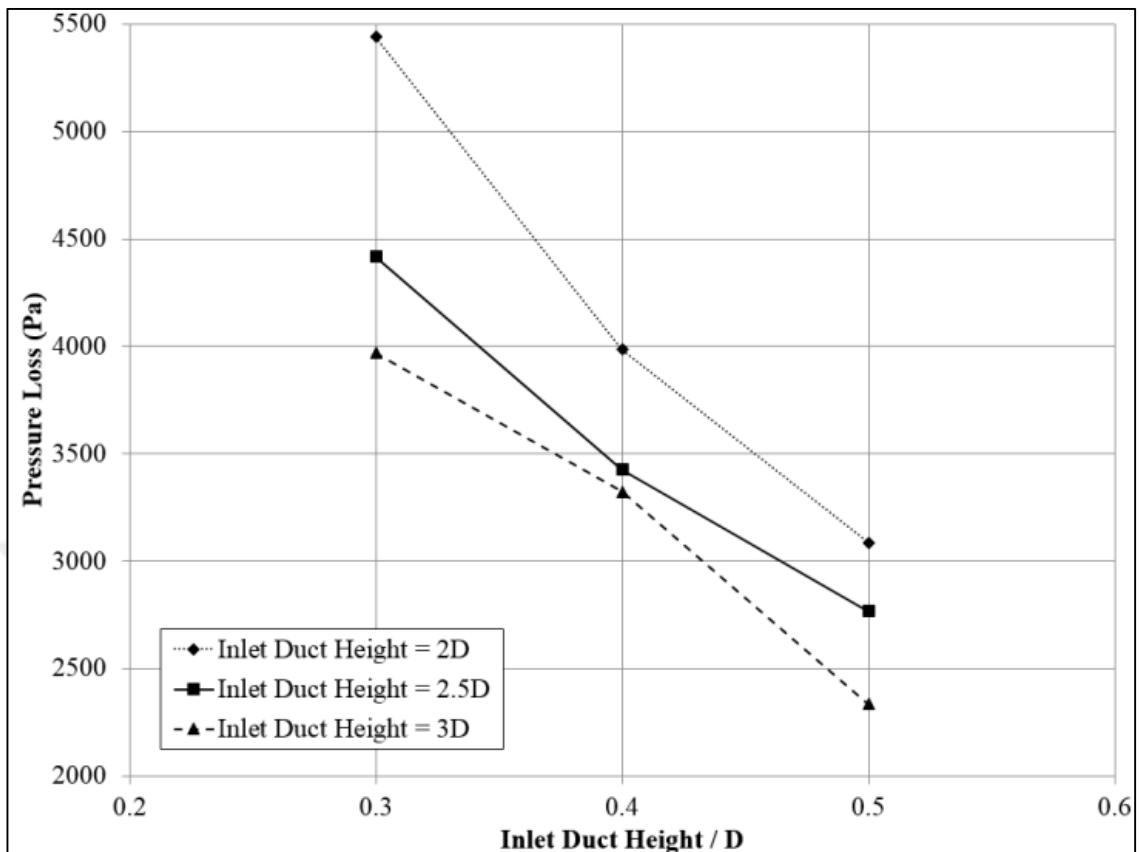


Figure 3.5. Pressure loss variations with different inlet duct height and swirl volume height

Inlet velocity of the cyclone is known to be effective for the separation performance. The higher inlet velocity causes an increase in the breakup rate of the particles. The lower inlet velocity slows down swirling flow yielding decrease in centrifugal force effect on the particles and decrease in the separation performance. Cyclone height is another effective parameter for the separation; it basically defines the end plane of the swirling flow. The particles flow through the swirling flow and the particles crashes the oil surface at the end of the swirl; therefore, they would be trapped. If the cyclone height is too long, the swirl slows down and more particles start to discharge from the port. If the cyclone height is too low, there is not enough time for the particles to reach the cyclone surface because they must flow with swirl. The separation efficiency is calculated from equation (3.14) below which is a function of total mass of the particles at the inlet and outlet. As a result of breakup and coalescence, the total number of particles in the flow volume may change.

$$\text{eff} = \frac{m_{\text{in}} - m_{\text{out}}}{m_{\text{in}}} \quad (3.14)$$

Figure 3.6 shows the change in the separation efficiency along with inlet duct height. It is noticed that while the cyclone height is increasing from 3D to 2D, separation performance seems to be increasing as well. On the other hand, for each swirl volume height, separation performance shows a decline when inlet duct height is increased. In other words, Figure 3.6 illustrates that when the inlet diameter decreases, the separation performance shows an increase. Therefore, the separation efficiency increase is inversely proportional with the decreasing inlet area.

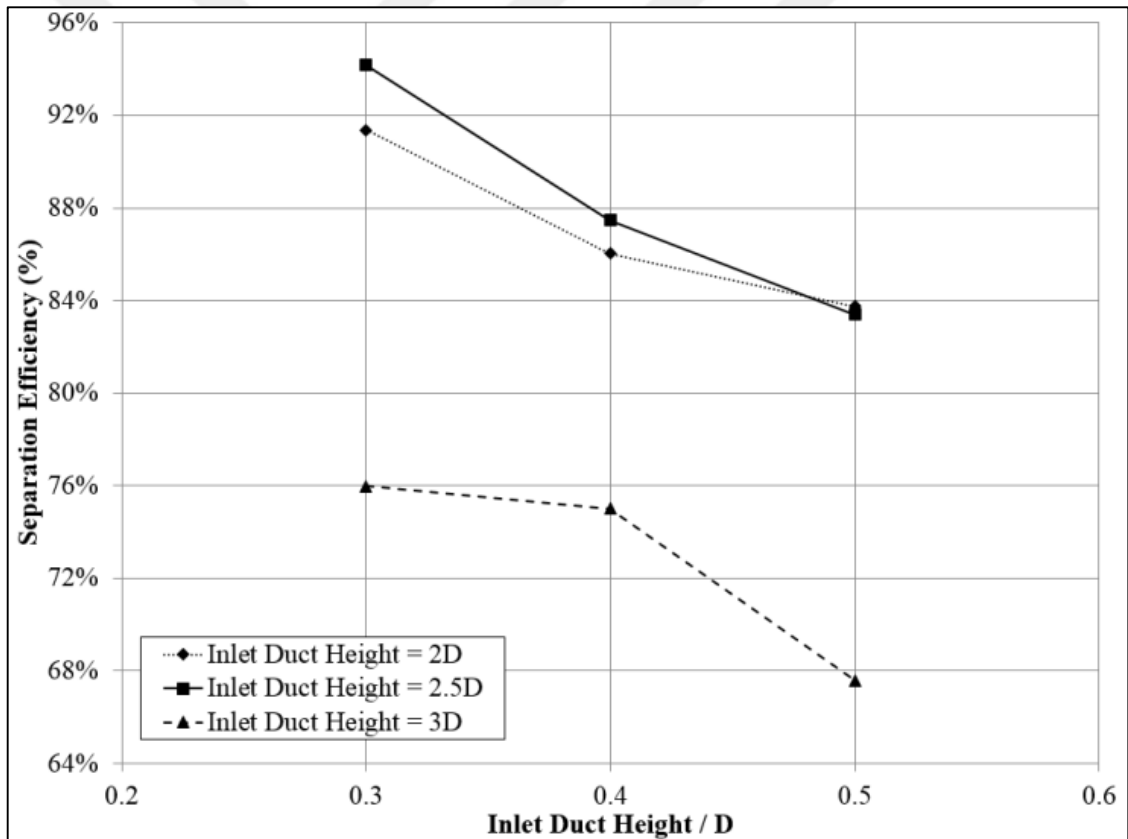


Figure 3.6. Separation efficiency with different inlet duct height and swirl volume height

4. INVESTIGATION OF VORTEX FINDER LOCATION EFFECTS ON ENERGY AND SEPARATION EFFICIENCY ON HYDROCYCLONES

Hydrocyclone separators are commonly used in chemical and energy industries for their advantages related to their simple manufacturing process and nearly maintenance-free specifications. The efficiency of hydrocyclones plays a considerable role in the overall system efficiency [61]. To observe the air flow inside the hydrocyclones, there are a lot of studies in literature. Neither experimental nor simulation results for cyclone flow observation are easy to achieve because of the fact that the flow is quite chaotic and cannot be observed with cross sections. Latest developments in CFD (Computational Fluid Dynamics) simulation enable researchers to understand the cyclone flow well.

There are more articles about cyclones than hydrocyclones. The main difference between cyclones and hydrocyclones is that hydrocyclones separate liquid particles from gas whereas cyclones separate solid particles from gas. While examining the separation process in hydrocyclones, there are many different physical phenomena to be observed. During this process, liquid particles can be broken up, merged or reshaped whereas solid particles cannot. Another specification of the liquid particles is that if a liquid particle gets close enough to the surface, it can stick to the surface; or if the surface flow speed increases over specific limit velocity, liquid particle separates from surface and starts to flow in main gas flow [62]. Therefore simulation of hydrocyclones is more complicated than the simulation of cyclones [21].

In this study, the effects of vortex finder location on horizontal positions of hydrocyclones were observed with CFD simulation. Commonly, hydrocyclones are manufactured with concentric vortex finder with main body. The hydrocyclone has been simulated with 4 different out-off-center vortex finder positions. The simulation shows that the eye wall of vortex flow takes the form of “S” letter. The flow profile of out-off-center is more chaotic than standard hydrocyclone simulations.

4.1. GEOMETRY OF SIMULATED VORTEX FINDER POSITIONS

Main parts of a hydrocyclone can be identified as main body, tangent inlet port and center outlet port channel, and vortex catcher oil surface [63]. The dimension of the outlet port channel has an important role in the separation and energy efficiency. The height and diameter effects have been discussed in previous chapters. In this chapter, the effects of the off-centered outlet channel will be reviewed. Outlet channel is moved to 4 different locations which are 3 mm away from the center (Figure 4.1). Model verification is performed in outlet channel on centered position.

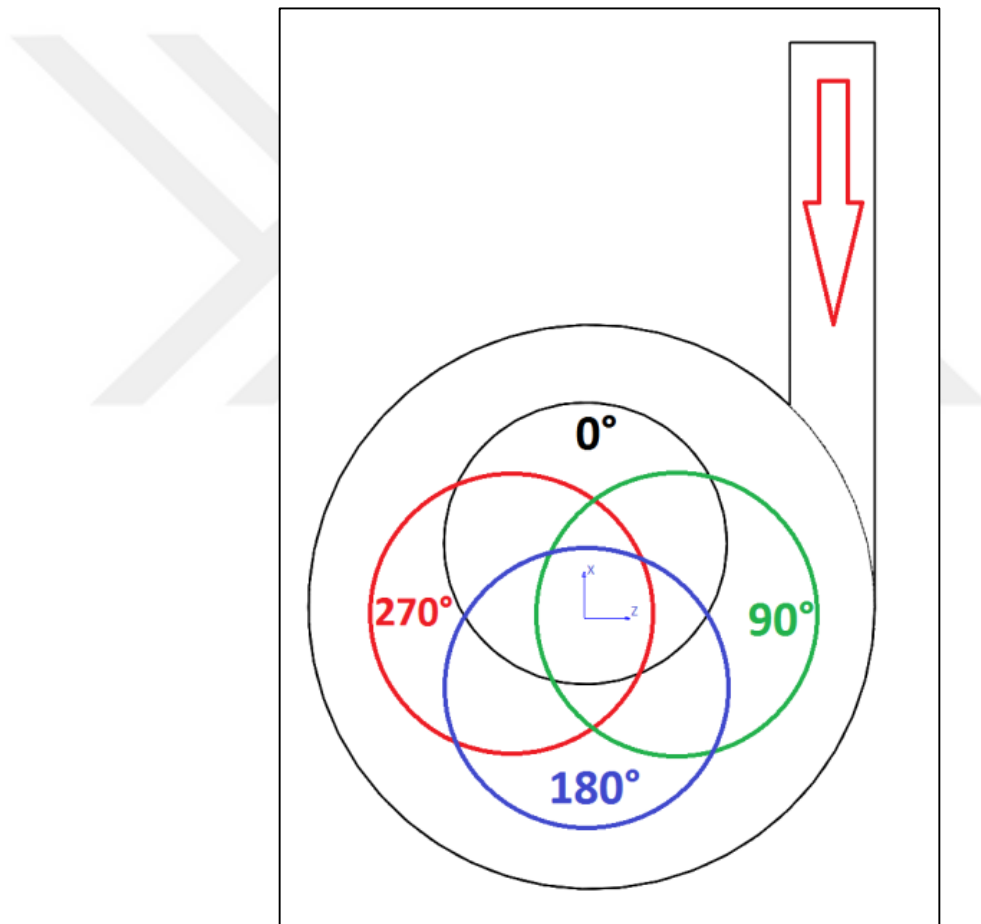


Figure 4.1. Separation efficiency with different inlet duct and swirl volume height

Table 4.1. Parameters of Oil Separation Tank

Hydrocyclone Height (H)		3D
Inlet channel dimensions	Height (a)	0.5D

	Width (b)	0.15D
	Area (a*b)	0.075D
	Channel length(L)	D
Vortex finder channel	Diameter (d)	0.5D
	Length (h)	D
Diameter of channel (D)		D
Center deviation of vortex finder	For 0°	0.004D
	for 90°	0.04D
	for 180°	0.04D
	for 270°	0.04D

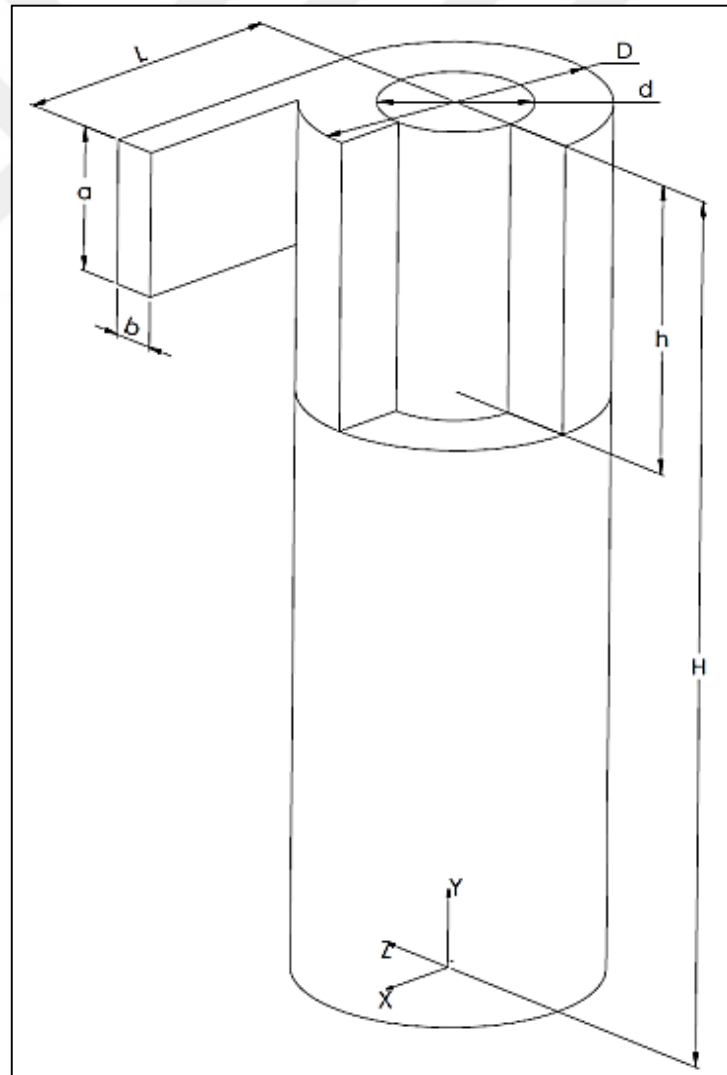


Figure 4.2. Parameters of oil tank geometry

The separator shown in Figure 4.2 was modelled parametrically with Solidworks by using the parameters indicated in Table 4.1. Then flow volume of separator was meshed with tetra meshes by automatic ICEM-CFD module. Because of high turbulence flow regime, polyhedral meshes give more consistent results. Therefore, tetra meshes are converted to polyhedral meshes in FLUENT (Figure 4.3) (Table 4.2).

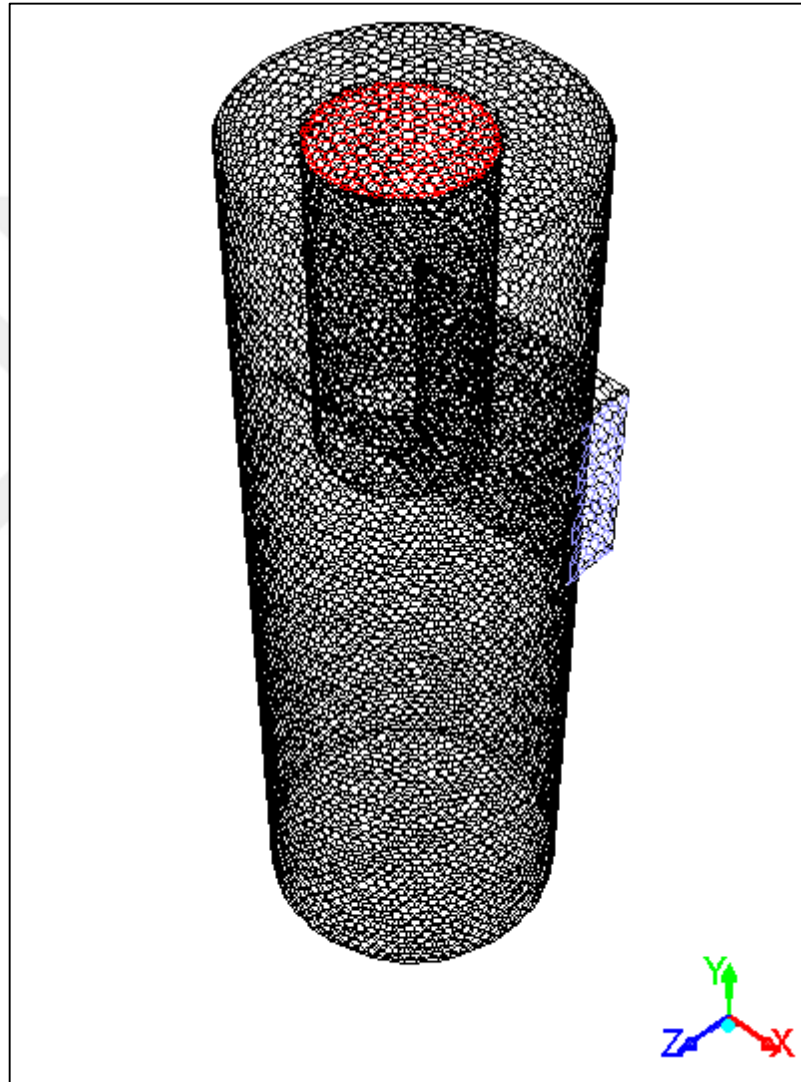


Figure 4.3. Mesh Overview

Grid independency is checked and tabled below. Pressure loss difference between coarse and fine mesh is only %5.

Table 4.2. Grid independency check results

Grid Independency Check Results	
Number of cells	Total pressure loss of oil tank(Pa)
33490	5544
51694	5548
90632	5826
Difference between finest and coarsest mesh (%)	5%

Table 4.3. Number of meshes

Number of meshes	
Number of tetrahedral premeshes	239790
Number of polihedral meshes	51698

As boundary conditions, inlet surface is defined by velocity inlet BC and outlet surface is defined by pressure outlet BC. All the walls are considered to be in a nonslip wall condition. Boundary conditions for DPM method have different specifications. Walls are assigned to wall film model except for the bottom wall which is specified as trap condition. Inlet and outlet surfaces are defined as escape boundary condition. This means that if a particle collides to the bottom wall it will be trapped by this wall; however, if it goes through the inlet or outlet surfaces, it is assumed to be escaped or cannot be separated. There is a gravity force of 9.81 m/s^2 in -y direction.

The specifications of oil and air in condition of separator inside; air density is 7.11 kg/m^3 and its viscosity is $18.5\text{E-}6 \text{ kg/m.s}$ at 298 K under 6.1 bar pressure; oil density is 832 kg/m^3 and its viscosity is $2.09\text{E-}6 \text{ kg/m.s}$. Surface tension of an oil droplet in these conditions is 0.056 n/m .

Three main assumptions have been made in this study. The first one is that although inlet port usually has a circular cross section shape, it is modelled as rectangular duct shape. The second one is that in real conditions, oil surface is always waving because of the air flow inside the separator. In this simulation, oil surface is modelled like a flat surface. And the

last assumption is related to the shape of oil particles. In reality, oil particles have a shape like a droplet and they can change their shape themselves. But the shape of oil particles is modelled as spherical and their shape never changes.



4.2. NUMERICAL MODEL

As a result of the importance of shear stress forces of flow in cyclones, Reynolds Stress Model (RSM) has been preferred in this study. RSM model increases the required solution time, but it gives more accurate results for this type of flows. For the liquid particles, Discrete Phase Model (DPM) was used. The results were corroborated with the comparison of the experimental results. The results showed that the effects of the vortex finder position are significant regarding to the separation and pressure loss efficiency. The most efficient position is observed when the vortex finder was positioned close to the main body interior wall near inlet port.

The solver model settings are referenced from the study of Kaya and Karagöz. Regarding the solver models, PRESTO model was used for pressure, SIMPLEC model was preferred for velocity and QUICK was utilized for momentum. A second degree solver was used for turbulence kinetic energy solution and the first degree solver was used for RSM model. Particles were modelled with DPM (Discrete Phase Model) and as sub models of DPM, Saffman Lift Force, Discrete Random Walk (DRW), Breakup, Stochastic Collision and Coalescence models were also used.

Normally, air flow has effects on the oil particles and vice versa. As the volumetric fraction of the oil particles is less than 10-12%, oil particles' effect on air flow was ignored for this simulation.

4.3. SIMULATION RESULTS

Model verification has been performed in the previous chapter. According to this verification, simulation results has an acceptable error rate with respect to the experimental results.

The results show that the different locations of the vortex finder cause changes in velocity and pressure profile, especially around the vortex finder. The velocity profile is the most important part for a cyclone separator. If there is a sudden increase in the velocity, the particles may split into smaller particles. Velocity magnitude should always be in the range of 14-21 m/s.

The contours of the velocity magnitude of a cross sectional horizontal plane on the center of inlet port do not show uniform velocity profiles for different vortex finder positions. The

most uniform profile is observed in vortex finder's 0° position. The reason of this uniformity can be explained with the effects of two different forces on the flow, one of these forces being the rotational flow and the other one as the inlet flow. They meet near after inlet port, so the velocity of the flow increases near this area. Therefore, the cross-sectional section of flow near this area can be expanded so as to decrease the velocity to an average magnitude. The velocity contours are shown only on a 2D plane, in fact the model was performed with 3D. The increments in velocity magnitude mix the flow or cause reverse flows in the vortex in cyclone separator. It can be calculated that catching a smooth flow profile is very important.

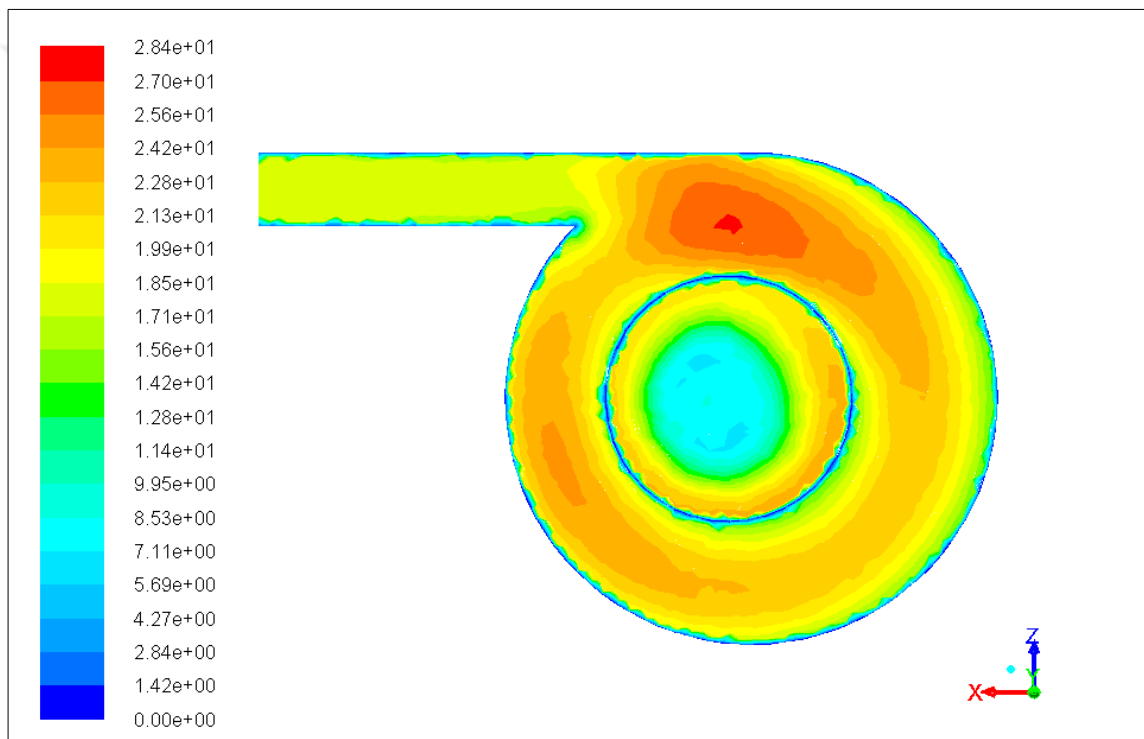


Figure 4.4. Contours of velocity magnitude (m/s) at 0° vortex finder position

In this study, the worst case is when the vortex finder is at 180° (Figure 4.5), since the cross-section of the flow volume was the narrowest, which is something that wasn't expected. Besides, some high velocity areas were observed. Moreover, the particles touched the outer wall in the high velocity location. And as a result of the high velocity, they can collide elastically and separated from the wall.

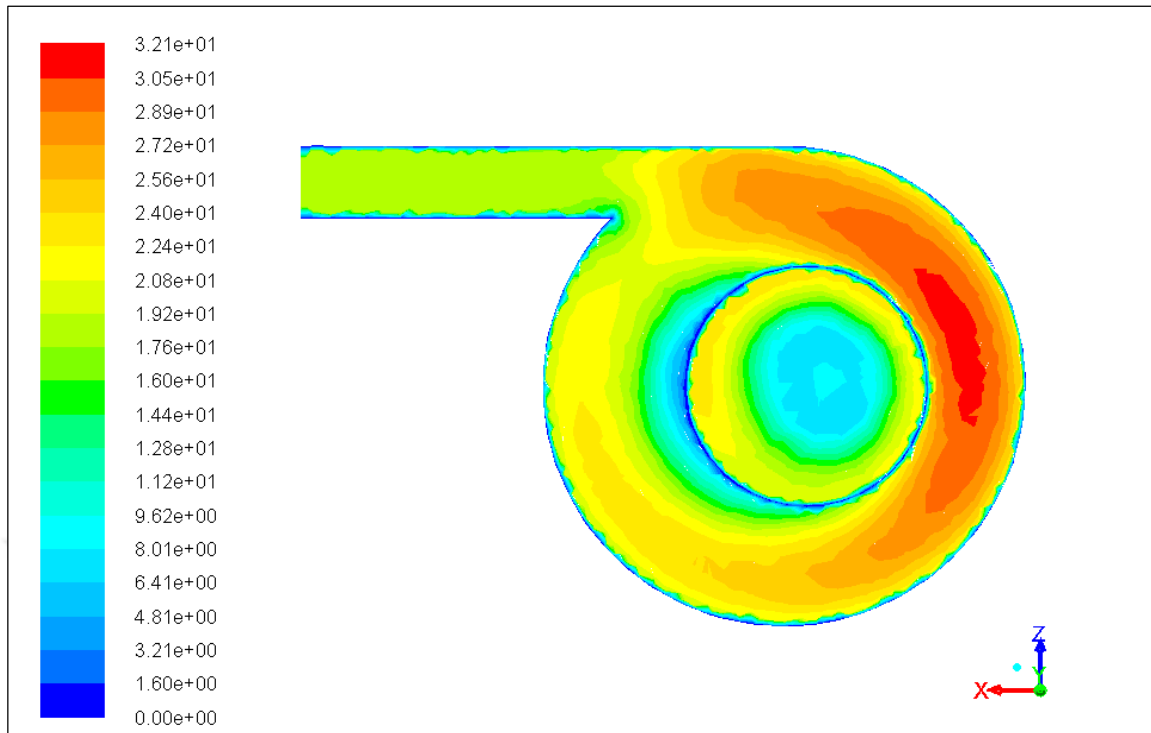


Figure 4.5. Contours of velocity magnitude (m/s) at 180° vortex finder position

On the other hand, non uniform velocity profile causes higher pressure loss in the system as a result of mixing smooth swirl flow profile.

For two other cases, where the vortex finder is at 90°(Figure 4.6) and 270°(Figure 4.7), the flow behaves different from other cases. The flow profile of 90° positioned vortex finder shows that there is a high velocity near inlet port. This sudden change in velocity can be used for improving the separation performance. However, if the velocity near inlet port is higher than it should be, it can affect the separation efficiency in a negative manner.

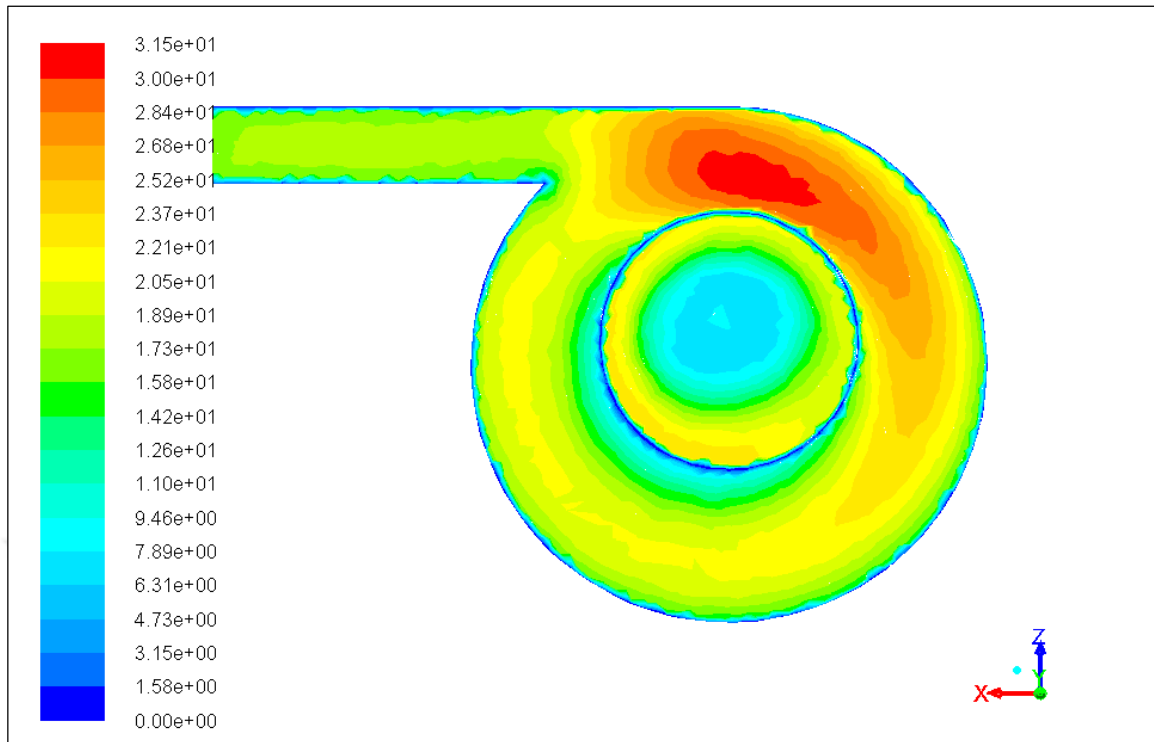


Figure 4.6. Contours of velocity magnitude (m/s) at 90° vortex finder position

At 270° (Figure 4.7) vortex finder, the sudden increase in the velocity magnitude is observed after the particles touch to the wall. This condition may cause the particles to leave from the wall.

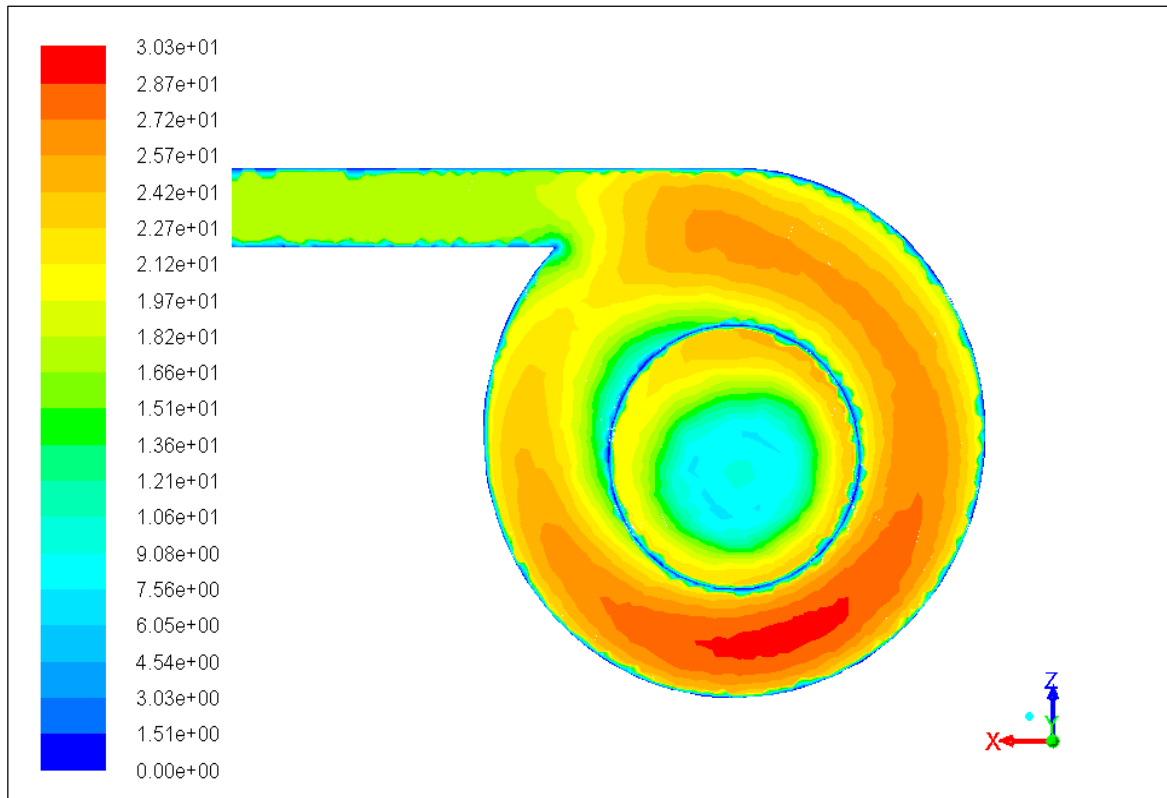


Figure 4.7. Contours of velocity magnitude (m/s) at 270° vortex finder position

Overall efficiency of the separator can be observed from the inlet and outlet values. The difference between the total pressure of inlet and outlet ports shows that the 0°(Figure 4.4) vortex finder position has the lowest pressure loss values and the highest values are at 270°(Figure 4.7) position. The reason can be predicted from the fact that the highest average velocity is observed at 270° vortex finder position. Although the highest velocities are observed at 180° position, the average values are more dominant for pressure loss.

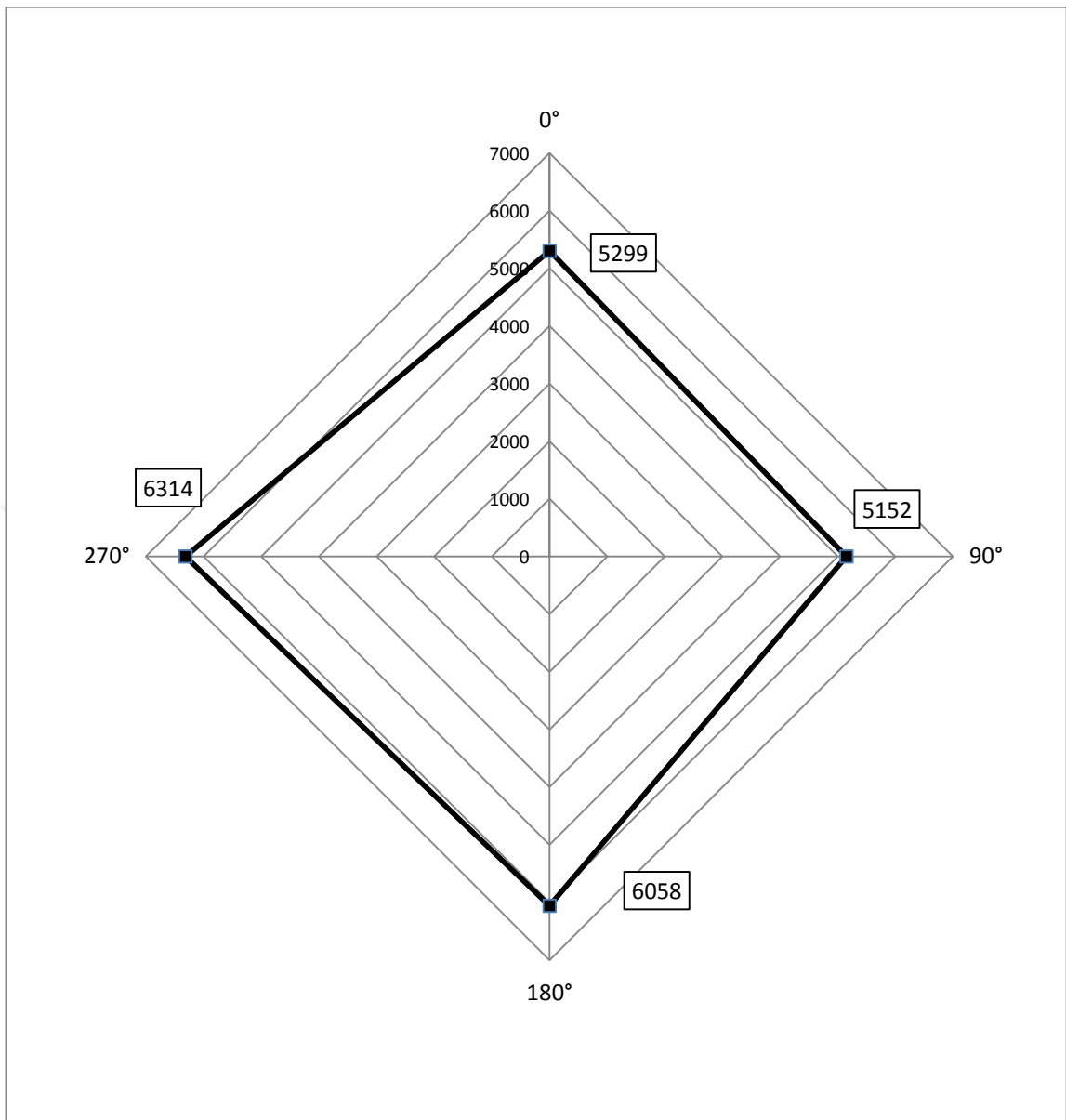


Figure 4.8. Pressure loss values for different off centred vortex positions

When the pressure loss and separation curves are compared, they look like proportional at first sight, but they are not. There are a lot of dependencies for the separation efficiency, so it is not possible to classify separation curves as dependent only to pressure loss curves. Separation efficiency graph shows that the maximum efficiency is achieved at 0° vortex finder position (Figure 4.8). This shows that if there is no sudden changes in flow velocity, the separation performance of a cyclone may increase (Figure 4.9).

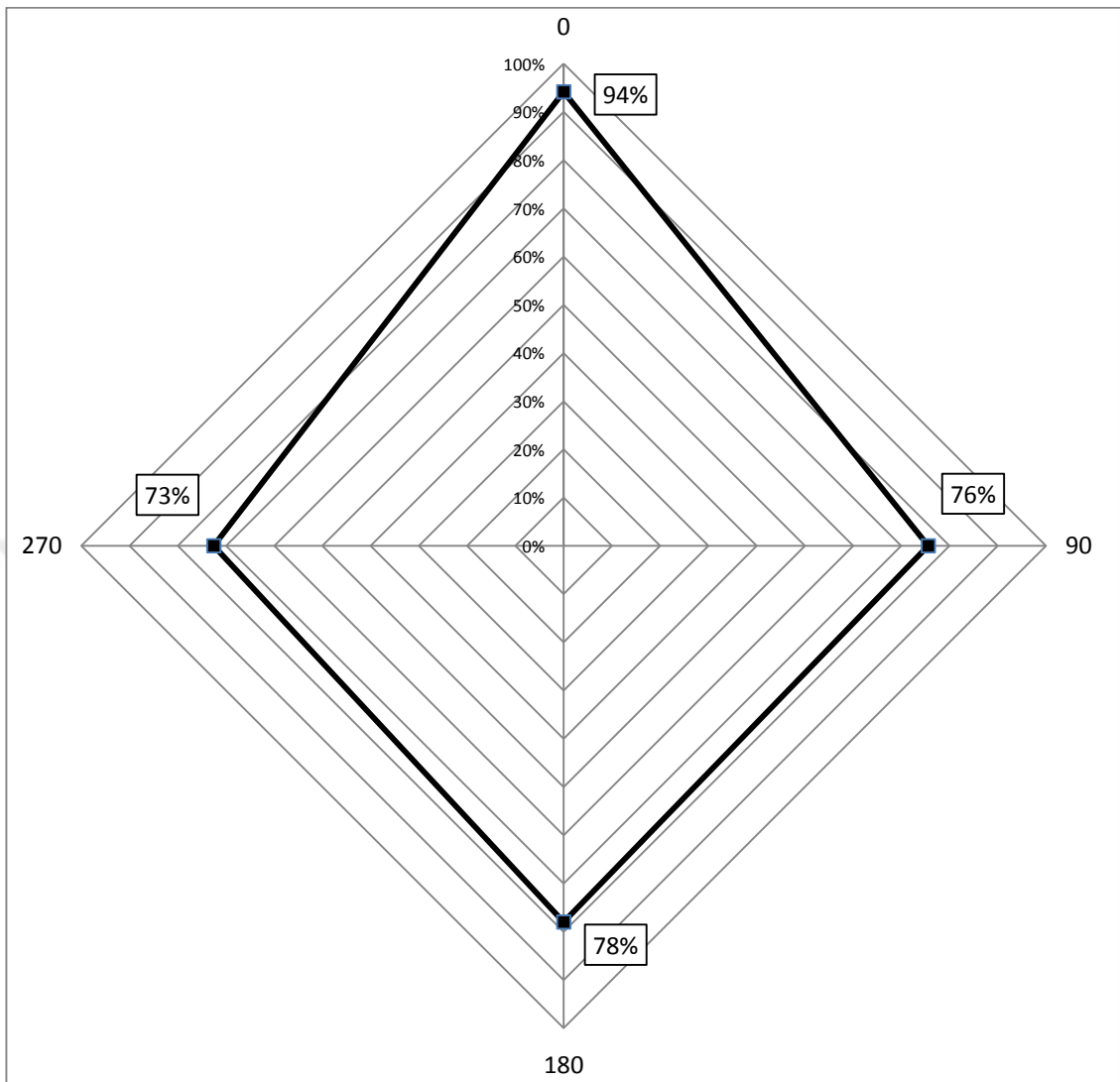


Figure 4.9. Particle separation efficiency values for different off centred vortex positions

5. CONCLUSIONS

The most important unit for energy efficiency of a screw compressor is air end performance. Leading factors on air end performance are related to the rotor and casing design. Rotor design is the subject of another study. But for the casing design, oil injection flow rate, oil injection point locations and dimensions have to be calculated accurately. If there is an error in the oil injection system calculations, air will be pressurized inefficiently and unfortunately the energy consumption rate of the compressor will increase.

Oil injection flow rate depends on the air flow rate. Therefore, oil injection changes proportional to the air flow capacity of a compressor. Generation of a formula for the exact calculation of oil flow rate is not possible. Because thermodynamic calculations focus only on the cooling balance between air and oil. These calculations ignore the oil stacking situation in the air end like a gearbox. For this reason, these calculations constitute only initial points for experimental studies.

Oil injection port locations are critical because the residual time of injected oil is as short as 0.005 seconds. If the injection ports are very close to the inlet port, air temperature starts to increase instead of decreasing. On the contrary, if they are too far to the inlet port, enough heat transfer between air and oil cannot be made. Thereby, heat energy of air cannot completely be transferred to oil. Oil injection flow rate depends on the suction air temperature and oil injection temperature.

In order to estimate the diameter of an oil injection port, firstly the oil injection flow rate and port locations must be calculated. Diameter estimation is directly correlated to the particle breakup theory; for this reason, chamber pressure and particle speed are main parameters for this calculation. Wide hole diameter results with bigger particles. Due to their heaviness, bigger particles directly stick to rotors and cannot perform an efficient cooling. On the other hand, small holes throw small particles out affecting the centrifugal force of air flow. They directly stick to the inner surface of the casing. They cannot cool the air efficiently. To catch an optimum diameter is essential for the air end design.

The optimum point of the separation performance is found to be related to the velocity and the flow angles in a cyclone. There are many parameters that can change the flow velocity

and flow angles. Therefore, more reliable results can be achieved by performing experiments or simulations as to the prediction of the relation between cyclone geometry and performance.

The height of a cyclone seems to be a significant parameter for the separation efficiency and energy consumption. It was noted that while the height is decreasing, the pressure loss increased. Another important point is that if the cyclone height is too short, the oil below the tank may be suctioned to the outlet port as a result of the low pressure area in the middle of the cyclone. This effect cannot be observed in this study because the oil surface below the tank was assumed to be flat .

Also, the change in the inlet port diameter seems to be affecting the separation efficiency as well. Specifically, inlet port diameter's influence on the short cyclones were more than long ones. In short cyclone geometry, the particles are trapped at the bottom surface because the swirl changes the direction from downward to upward more sharply in close of bottom trap condition surface. The particles cannot hang on the multiphase flow due to sharp turns and they separate. When the bottom surface is closer to the inlet port, differences between the downward and upward velocities are faster than the inlet velocity near the bottom surface, thus increasing the sharp turn effect.

While the inlet diameter is getting smaller, the separation performance increases the efficiency. Because the high velocity inlet provides more efficient separation, the inlet velocity shows an increase and the breakup possibility of the particles also increases yielding to separate particles with 10^{-5} mm diameter.

For the future work, if enough budget is provided, the results will be validated with experiments for airend and oil separation tank. Both components requires expensive test equipment for experiments. For oil separation tank, a particle diameter analyser must be provided. Besides, in order to make an iterative study, there is a need for a high budget in order to manufacture oil separation tanks in different dimensions. Requirements are also valid for the airend. Moreover, a bare screw compressor unit cannot be simulated with an acceptable error rate with today's simulation software. Nowadays there are some studies regarding to the basic airend simulation. If the experiments can be performed with a test rig, these basic airend simulation techniques can be performed and some comparison may be made with the obtained test results.

REFERENCES

1. H. Lund and G. Salgi, The Role of Compressed Air Energy Storage (CAES) in Future Sustainable Energy Systems, *Energy Conversion and Management*, 5:1172–1179, 2009.
2. C. Burgess, Energy Efficient Compressed Air Systems, *Energy in Buildings and Industry*, 25–28, 2008.
3. O. M. Al-Rabghi, M. H. Al-Beirutty, and K. A. Fathalah, Estimation and Measurement of Electric Energy Consumption due to Air Conditioning Cooling Load, *Energy Conversion and Management*, 14:1527–1542, 1999.
4. A. Almad, Choosing Oil-Injected Screw Compressors, *Chemical Engineering*, 2:35–39, 2012.
5. C. J. B. Dicken and W. Merida, Temperature Distribution within a Compressed Gas Cylinder during Fast Filling, in *Thermec 2006 Supplement: 5th International Conference On Processing And Manufacturing Of Advanced Materials*, pages 281–286, 2007.
6. J. Bartos, Understand Compressor Types to Make the Right Selection, *Plant Engineering*, 1:42–45, 2006.
7. S. Sapmaz, F. Kilic, M. Eyidogan, O. Taylan, V. Coban, S. Cagman, I. Kilicaslan, and D. Kaya, Selection of Compressors for Petrochemical Industry in Terms of Reliability, Energy Consumption and Maintenance Costs Examining Different Scenarios, *Energy, Exploration and Exploitation*, 1:43–62, 2015.
8. T. Giampaolo, *Compressor Handbook Principles and Practice*. 2010.
9. W. E. Bill Forsthoffer, Screw Compressors, in *Forsthoffer's Rotating Equipment Handbooks*, 371–392, 2005.
10. C. Liu, D. Kong, and M. Cai, Research on Energy-Saving Operation of Screw Air

Compressor, *Energy Education Science and Technology Part A: Energy Science and Research*, 1:355–360, 2013.

11. H. Tanaka, Y. Kamiya, M. Takano, and T. Nozaki, Oil Injection Rotary Screw Compressors Contributing to Environmental Protection and Energy Conservation, *Hitachi Review*, 5:245–249, 2011.

12. J. Feng, Y. Chang, X. Peng, and Z. Qu, Investigation of the Oil–gas Separation in a Horizontal Separator for Oil-Injected Compressor Units, *Proceedings of the Institution of Mechanical Engineers, Part A: Journal of Power and Energy*, 4:403–412, 2008.

13. C. A. I. Ferreira, C. Zamfirescu, and D. Zaytsev, Twin Screw Oil-Free Wet Compressor for Compression-Absorption Cycle, *International Journal of Refrigeration*, 4:556–565, 2006.

14. Y. Zhao, L. Li, H. Wu, and P. Shu, Theoretical and Experimental Studies of Water Injection Scroll Compressor in Automotive Fuel Cell Systems, *Energy Conversion and Management*, 9–10:1379–1392, 2005.

15. J. Shen, Z. Xing, K. Zhang, Z. He, and X. Wang, Development of a Water-Injected Twin-Screw Compressor for Mechanical Vapor Compression Desalination Systems, *Applied Thermal Engineering*, 125–135, 2016.

16. J. Li, H. Wu, B. Wang, Z. Xing, and P. Shu, Research on the Performance of Water-Injection Twin Screw Compressor, *Applied Thermal Engineering*, 16:3401–3408, 2009.

17. A. Lundberg, Screw Compressor Packages, *Australian refrigeration, Air conditioning and heating*, 9:22–24, 26, 28, 1985.

18. S. V. Krichel and O. Sawodny, Dynamic Modeling of Compressors Illustrated by an Oil-Flooded Twin Helical Screw Compressor, *Mechatronics*, 1:77–84, 2011.

19. T. U. Jung, S. H. Lee, S. Il Kim, S. J. Park, and J. P. Hong, The Development of

Hybrid Electric Compressor Motor Drive System for HEV, in *VPPC 2007 - Proceedings of the 2007 IEEE Vehicle Power and Propulsion Conference*, pages 802–807, 2007.

20. E. Chukanova, N. Stosic, and A. Kovacevic, *Numerical Analysis of Unsteady Behaviour of a Screw Compressor Plant System*. 2013.

21. N. Seshaiyah, S. K. Ghosh, R. K. Sahoo, and S. K. Sarangi, Mathematical Modeling of the Working Cycle of Oil Injected Rotary Twin Screw Compressor, *Applied Thermal Engineering*, 1:145–155, 2007.

22. M. Fujiwara and Y. Osada, Performance Analysis of an Oil-Injected Screw Compressor and Its Application, *International Journal of Refrigeration*, 4:220–227, 1995.

23. N. Stosic, I. K. Smith, and A. Kovacevic, Optimisation of Screw Compressors, *Applied Thermal Engineering*, 10:1177–1195, 2003.

24. X. Gao, J. Chen, J. Feng, and X. Peng, Numerical and Experimental Investigations of the Effects of the Breakup of Oil Droplets on the Performance of Oil-Gas Cyclone Separators in Oil-Injected Compressor Systems, *International Journal of Refrigeration*, 7:1894–1904, 2013.

25. E. W. C. Lim, Y. R. Chen, C. H. Wang, and R. M. Wu, Experimental and Computational Studies of Multiphase Hydrodynamics in a Hydrocyclone Separator System, *Chemical Engineering Science*, 24:6415–6424, 2010.

26. A.J.Hoekstra, Gas Flow Field and Collection Efficiency of Cyclone Separators, 2000.

27. J. Gimbut, CFD Simulation of Aerocyclone Hydrodynamics and Performance at Extreme Temperature, *Engineering Applications of Computational Fluid Mechanics*, 1:22–29, 2008.

28. K. Nageswararao, D. M. Wiseman, and T. J. Napier-Munn, Two Empirical Hydrocyclone Models Revisited, in *Minerals Engineering*, 5:671–687, 2004.

29. J. Gimbut, T. G. Chuah, T. S. Y. Choong, and A. Fakhru'l-Razi, A CFD Study on the Prediction of Cyclone Collection Efficiency, *International Journal for Computational Methods in Engineering Science and Mechanics*, 3:161–168, 2005.
30. F.Kaya and I.Karagöz, Performance Analysis of Numerical Schemes in Highly Swirling Turbulent Flows in Cyclones, *Current Science*, 95:1273-1278, 2008.
31. G. Gronald and J. J. Derksen, Simulating Turbulent Swirling Flow in a Gas Cyclone: A Comparison of Various Modeling Approaches, *Powder Technology*, 1–3:160–171, 2011.
32. W. P. Adamczyk, A. Klimanek, R. A. Bialecki, G. Wucel, P. Kozoub, and T. Czakiert, Comparison of the Standard Euler-Euler and Hybrid Euler-Lagrange Approaches for Modeling Particle Transport in a Pilot-Scale Circulating Fluidized Bed, *Particuology*, 129–137, 2014.
33. R. Utikar, N. Darmawan, M. Tade, Q. Li, G. Evans, M. Glenney, and V. Pareek, Hydrodynamic Simulation of Cyclone Separators, *Computational Fluid Dynamics*, January: 241–266, 2010.
34. N. Zeoli and S. Gu, Numerical Modelling of Droplet Break-up for Gas Atomisation, *Computational Materials Science*, 2:282–292, 2006.
35. S. Noroozi and S. H. Hashemabadi, CFD Simulation of Inlet Design Effect on Deoiling Hydrocyclone Separation Efficiency, *Chemical Engineering and Technology*, 12:1885–1893, 2009.
36. K. Yetilmezsoy, Determination of Optimum Body Diameter of Air Cyclones Using a New Empirical Model and a Neural Network Approach, *Environmental Engineering Science*, 4:680–690, 2006.
37. T. C. Rao, K. Nageswararao, and A. J. Lynch, Influence of Feed Inlet Diameter on the Hydrocyclone Behaviour, *International Journal of Mineral Processing*, 4:357–363, 1976.

38. M. Fujiwara, Kasuya.K, T. Matsunaga, and M. Watanabe, Computer Modeling for Performance Analysis of Rotary Screw Compressor, 1984.
39. N. Seshaiyah, S. K. Ghosh, R. K. Sahoo, and S. K. Sarangi, Performance Analysis of Oil Injected Twin Screw Compressor,*18th National and 7th ISHMT-ASME Heat and Mass Transfer Conference*, 1261–1268, 2006.
40. N. Isshiki, Theoretical and Experimental Study on Atomization of Liquid Drop in High Speed Gas Stream,*Transportation Technical Research Institute Technical Report 35*, 1959.
41. O. F. P. Lyons, C. Quinn, T. Persoons, and D. B. Murray, Heat Transfer and Flow in an Atomizing Mist Jet: A Combined Hot Film and Shadowgraph Imaging Approach,*Journal of Physics: Conference Series*, 1:12173, 2012.
42. D. Zaytsev and C. A. I. Ferreira, Profile Generation Method for Twin Screw Compressor Rotors Based on the Meshing Line,*International Journal of Refrigeration*, 5:744–755, 2005.
43. J. Do Suh and D. G. Lee, Manufacture of Composite Screw Rotors for Air Compressors by RTM Process, in *Journal of Materials Processing Technology*, 1–3:196–201, 2001.
44. N. Stošić, L. Milutinović, K. Hanjalić, and A. Kovačević, Investigation of the Influence of Oil Injection upon the Screw Compressor Working Process,*International Journal of Refrigeration*, 4:206–220, 1992.
45. N. Stosic, On Heat Transfer in Screw Compressors,*International Journal of Heat and Fluid Flow*, 285–297, 2015.
46. K. A. Woodbury, R. P. Taylor, and G. P. Moynihan, A Transient Fluid And Thermodynamic Model Of A Compressed Air by Submitted in Partial Fulfillment of the Requirements for the Degree of Master of Science in the Department of Mechanical Engineering in the Graduate School of The University of Alabama TUSCA, 2011.

47. P. J. Singh and G. C. Patel, A Generalized Performance Computer Program for Oil Flooded Twin-Screw Compressors, 1984.
48. M. Pascu, D. Buckney, and G. Cook, Numerical Investigation Of The Leakage Flows In Twin Screw Compressor Rotors, in *International Compressor Engineering Conference*, 2014.
49. H. Wu, X. Peng, Z. Xing, and P. Shu, Experimental Study on P-V Indicator Diagrams of Twin-Screw Refrigeration Compressor with Economizer, *Applied Thermal Engineering*, 10:1491–1500, 2004.
50. A. Kovačević, N. Stošić, and I. K. Smith, Numerical Simulation of Combined Screw Compressor-Expander Machines for Use in High Pressure Refrigeration Systems, *Simulation Modelling Practice and Theory*, 8:1143–1154, 2006.
51. D. Guerrato, J. M. Nouri, N. Stosic, and C. Arcoumanis, Flow and Pressure Characteristics within a Screw Compressor, *Journal of Physics: Conference Series* 12012, 2007.
52. I. Zlatanović and N. Rudonja, Experimental Evaluation of Desuperheating and Oil Cooling Process through Liquid Injection in Two-Stage Ammonia Refrigeration Systems with Screw Compressors, *Applied Thermal Engineering*, 210–215, 2012.
53. M. De Paepe, W. Bogaert, and D. Mertens, Cooling of Oil Injected Screw Compressors by Oil Atomisation, *Applied Thermal Engineering*, 17–18:2764–2779, 2005.
54. M. Yang, B. Wang, X. Li, W. Shi, and L. Zhang, Evaluation of Two-Phase Suction, Liquid Injection and Two-Phase Injection for Decreasing the Discharge Temperature of the R32 Scroll Compressor, *International Journal of Refrigeration* 269–280, 2015.
55. Z. H. Fong, F. C. Huang, and H. S. Fang, Evaluating the Inter-Lobe Clearance of Twin-Screw Compressor by the Iso-Clearance Contour Diagram (ICCD), *Mechanism and Machine Theory*, 6:725–742, 2001.

56. J. S. Fleming and Y. Tang, The Analysis of Leakage in a Twin Screw Compressor and Its Application to Performance Improvement, *IMechE 1995*, 2:125–136, 1995.
57. P. Singh and J. Bowman, Heat Transfer in Oil-Flooded Screw Compressors, *International Compressor Engineering Conference*, pages 135–153, 1986.
58. X. Gao and J. Chen, Numerical and Experimental Investigations of the Effects of the Breakup of Oil Droplets on the Performance of Oil-Gas Cyclone Separators in Oil-Injected Compressor Systems, *Computer and Fluids*, 92:45–55, 2014.
59. T. Van Den Moortel, E. Azario, R. Santini, and L. Tadrist, Experimental Analysis of the Gas-Particle Flow in a Circulating Fluidized Bed Using a Phase Doppler Particle Analyzer, *Chemical Engineering Science*, 10:1883–1899, 1998.
60. O'Rourke and P.B., Modeling of Drop Interactions in Thick Sprays and a Comparison, *Proceedings of the Institution of Mechanical Engineers*, 101–106, 1980.
61. R. Cohen, Advances in Compressor Technology (as Reported in 1988), *International Journal of Refrigeration*, 4:274–277, 1990.
62. X. Gao, Y. Zhao, J. Feng, Y. Chang, and X. Peng, The Research on the Performance of Oil-Gas Cyclone Separators in Oil Injected Compressor Systems with Considering the Breakup of Oil Droplets, 2011:1–10, 2012.
63. W. Zhongyi, Y. Changlong, H. Jia, and Y. Yunliang, The Analysis of Internal Flow Field in Oil-Gas Separator, *Procedia Engineering*, 4337–4341, 2011.